Expected Grad-CAM: Towards gradient faithfulness

Vincenzo Buono

Halmstad University vincenzo.buono@hh.se

Peyman S. Mashhadi

Halmstad University peyman.mashhadi@hh.se

Mahmoud Rahat

Halmstad University mahmoud.rahat@hh.se

Prayag Tiwari
Halmstad University

Halmstad University prayag.tiwari@hh.se

Stefan Byttner

Halmstad University stefan.byttner@hh.se

Abstract

Although input-gradients techniques have evolved to mitigate and tackle the challenges associated with gradients, modern gradient-weighted CAM approaches still rely on vanilla gradients, which are inherently susceptible to the saturation phenomena. Despite recent enhancements have incorporated counterfactual gradient strategies as a mitigating measure, these local explanation techniques still exhibit a lack of sensitivity to their baseline parameter. Our work proposes a gradient-weighted CAM augmentation that tackles both the saturation and sensitivity problem by reshaping the gradient computation, incorporating two well-established and provably approaches: Expected Gradients and kernel smoothing. By revisiting the original formulation as the smoothed expectation of the perturbed integrated gradients, one can concurrently construct more faithful, localized and robust explanations which minimize infidelity. Through fine modulation of the perturbation distribution it is possible to regulate the complexity characteristic of the explanation, selectively discriminating stable features. Our technique, Expected Grad-CAM, differently from recent works, exclusively optimizes the gradient computation, purposefully designed as an enhanced substitute of the foundational Grad-CAM algorithm and any method built therefrom. Quantitative and qualitative evaluations have been conducted to assess the effectiveness of our method.¹

1 Introduction

In recent years, deep neural networks (DNNs) have consistently achieved remarkable performances across a rapidly growing spectrum of application domains. Yet, their efficacy is often coupled with a *black-box* operational behavior, commonly lacking transparency and explainability [43, 2]. Such challenges have catalyzed a shift towards the research and development of *Explainable AI* (xAI) methodologies, aimed at obtaining a deeper understanding of the intrinsic mechanisms and inner workings driving the model's decision processes [22]. Driven by the need for trustworthiness and reliability [33], numerous techniques, ranging from gradient-based [50], perturbation-based [39] and contrastive approaches [1], have emerged to assess *a posteriori* (post-hoc) the behavior of opaque models [44]. Within the branch of *visual explanations*, *saliency* methods aim to discriminate and identify relevant regions in the input space that highly excite the network and strongly influence the network predictions.

As successful state-of-the-art vision tasks' architectures commonly incorporate spatial convolution mechanism, *Class Activation Maps* (CAM) [61] have emerged as a popular and widely adopted technique for generating *saliencies* that leverage the spatial information captured by convolutional

¹Implementation available at https://github.com/espressoshock/pytorch-expected-gradcam.

layers. CAM(s) are computed by inspecting the feature maps and produce per-instance, class-specific attention heat maps that highlight important areas in the original image that drove the classifier. Building on this notion, Gradient-weighted CAM (Grad-CAM) [46] and its variants, extend the original formulation by computing the linear weights from the averaged backpropagated gradients w.r.t. target class of each feature map. This generalization enables the use and application of the method without any modification or auxiliary training to the model. Historically, naïve vanilla gradients have been cardinal in the development and evolution of saliency maps [50]; however input-gradients techniques (e.g. output gradients w.r.t. inputs) quickly evolved to address the gradient saturation problem [48, 38, 56], where the gradients of important features results in small magnitudes due to the model's function flattening in the vicinity of the input, misrepresenting the feature importance [55]. Within the context of gradient visualizations, several counterfactual-based works have been proposed in an attempt to address the saturation issue by feature scaling [56], contribution decomposition [48] and relevance propagation [10]. In this direction, the insensitivity of baselinemethods to their reference parameter [54, 3] has spurred an area of research dedicated to baseline determination [8, 29, 59]. Since the introduction of the original proposition of CAM and Grad-CAM, several gradient-based techniques have been proposed in an effort to improve localization [47, 27], multi-instance detection [13], saliency resolution [37, 16], noise and attribution sparsity [35] and axiomatic attributions [20]. Despite numerous techniques being presented to address the saturation phenomena, modern and widely adopted gradient-weighted CAM approaches still rely on vanilla gradients, which are inherently prone to gradient saturation. A recent work, namely Integrated Grad-CAM [45], has been proposed aimed to address this issue which combines two well-established techniques: Integrated Gradients and Grad-CAM. Nonetheless, this method retains the same shortcomings as its underlying parent approach, that is, its lack of sensitivity to its baseline parameter, which underestimates contributions that align with its baseline.

Following this research trajectory, we theorize and demonstrate that we can *concurrently* improve four explanation quality key desiderata in the context of human-interpretable saliencies [24, 25]: (i) fidelity, (ii) robustness, (iii) localization, and (iv) complexity. In this paper, we demonstrate that the explanations generated by our approach simultaneously satisfy many desirable xAI properties by producing saliencies that are highly concentrated (i.e. high localization↑) on the least number (low complexity↓) of stable (low sensitivity to infinitesimal perturbation) robust features (features which are consistently used). Our experiments reveal that Expected Grad-CAM significantly outperforms currently state-of-the-art gradient- and non-gradient-based CAM methods across the tested xAI metrics in a large evaluation study. The results are consistent across different open image datasets. Qualitatively, our technique constructs saliencies that are sharper (less noisy) and more focused on salient class discriminative image regions, as illustrated in fig. 1. Figure 4 shows that the saliency maps of popular gradient-based CAM methods are often noisy and appear sparse and uninformative [28], with large portions of pixels outside the relevant subject. In contrast, Expected Grad-CAM highlights only those features that systematically are utilized not only for a given sample but also for all the samples in its vicinity in the input space and thus, that produce the same prediction (i.e. relative input stability[4]).

Our method, *Expected Grad-CAM*, tackles the current limitations of existing methods by reshaping the original gradient computation by incorporating the provably and well-established *Expected Gradients* [18] difference-from-reference approach followed by a smoothing kernel operator (fig. 3). As opposed to prior methods, our work solves the underestimation of the feature attribution (fig. 2) without introducing undesired side effects (*i.e.* parameter insensitivity) by sampling the baseline parameter of the path integral from a reference distribution. As generated CAM(s) are coarse attention maps (*i.e.* inherently low complexity saliencies), they are often used with the end goal of *human-centered* interpretability of the function predictor and its behavior [6]. Therefore, it is crucial that such attribution methods highlight only stable features focusing only on salient areas of the original input [6].

We summarize our contributions as follows: first, we provide a general scoring scheme that is not bound along a monotonic geometric path for generating gradient class activation maps that minimize infidelity for arbitrary perturbations. Second, we propose Expected Grad-CAM, a gradient-weighted CAM augmentation that produces class-specific heat maps that simultaneously improve four modern key explanatory quality desiderata. Third, we evaluate the effectiveness of our approach on a large evaluation study across 19 quality estimators on recent explanation quality groupings [24, 25] *i.e.* (i)

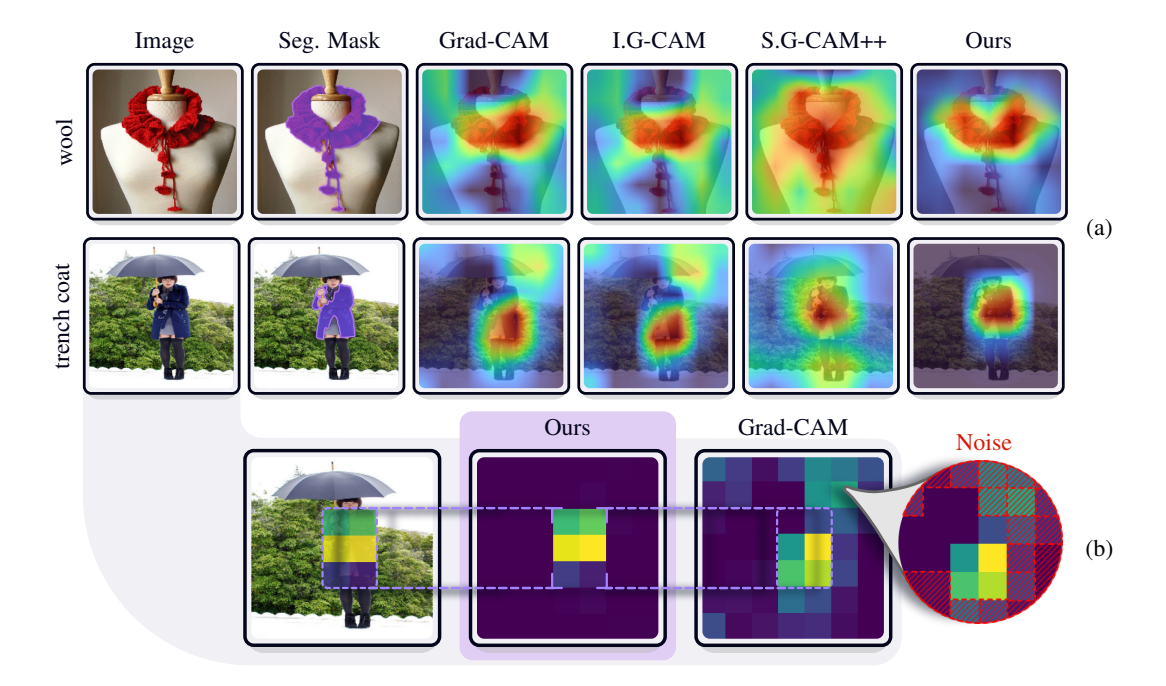


Figure 1: Explanatory functions on VGG-16 across samples from ImageNet-1k [42]. Our approach produces sharper (less noisy) and higher localized heat maps with lower complexity than existing methods (1a). Figure 1b shows the coarse heat map with respect to our method and baseline Grad-CAM [46].

Faithfulness, (ii) Robustness, (iii) Complexity, and (iv) Localization. Lastly, we demonstrate that our technique significantly outperforms state-of-the-art gradient- and non-gradient-based CAM methods.

2 Related work

The following section presents a brief discussion of prior attribution methods alongside their known shortcomings and notation.

Gradient-based explanations This set of techniques encompasses the involvement of the neural network's gradients as a function approximator, translating complex nonlinear models into local linear explanations. These explanations are often encoded as attention heat maps, also known as saliencies. The cornerstone method within this category is **Input-Gradients** (vanilla gradients) [50]. Consider a classical supervised machine learning problem, where $x \in \mathbb{R}^D$ be an input sample point for a neural network $F: \mathbb{R}^D \to \mathbb{R}^C$. The class-specific input-gradients, are the backpropagated gradients of the output w.r.t. the input sample and are defined as:

$$\phi_i(x; F^c) = \nabla_x F^c(x) \tag{1}$$

where $\phi_i(x; F^c)$ denotes the gradient of the class c w.r.t. the input x. Notably, while not relevant to our approach, the feature visualization produced by deconvolution [60] and guided backpropagation [53] are also tightly linked, with the latter letting flow only non-negative gradients.

Counterfactual explanations As gradients only express local changes, their utilization misrepresents feature importances across saturating ranges [56]. This class of methods tackles this issue by multiple nonlocal comparisons against a perturbed baseline by feature re-scaling [56], blurring [19], activation differences [48], noise [52] or inpainting [5]. Here, we primarily focus on two kinds of methods that are highly related to our work: Integrated Gradients [56] and SmoothGrad [52].

Integrated Gradients This method involves the summation of the (interior) gradients along the path of counterfactuals [56, 55]. It is defined as:

$$\phi_i^{IG}(x, x'; F^c) = (x - x') \int_{\alpha=0}^1 \nabla_x F^c \left(x' + \alpha \left(x - x' \right) \right) d\alpha \tag{2}$$

where x is the input sample, x' is a given baseline, F^c is the neural network output for class c, and α is a scaling parameter that interpolates between the baseline and the input according to a given interpolation function γ [56].

SmoothGrad: This method addresses saliency noise caused by sharp fluctuations of gradients at small scales, due to rapid local variation in partial derivatives [52], by denoising using a smoothing Gaussian kernel. It is defined as:

$$\phi_i^{SG}(x; F^c) = \frac{1}{n} \sum_{1}^{n} \nabla_x F^c \left(x + \mathcal{N} \left(\overline{0}, \sigma^2 \right); F^c \right) \tag{3}$$

where x is the input sample, $\mathcal{N}(\overline{0}, \sigma^2)$ is Gaussian noise with mean 0 and variance σ^2 , F^c is the neural network output for class c, and n is the number of noisy samples averaged.

Class activation mapping This set of attention methods generates explanations by exploiting the spatial information captured by the convolutional layers. Class activation maps are generated by computing the rectified sum of all the feature map's activations times its weights. Formally, consider a network's target convolutional layer output having size s and let $f_{x,y}^k \in \mathbb{R}$ be the activation of unit k in the target convolution layer at spatial location (x,y). Then the class activation map [61] for class c at spatial location (x,y) are computed as

$$M_{x,y}^c = \sum_k w_k^c f_{x,y}^k \tag{4}$$

where $w \in \mathbb{R}^k$ are the weights of the fully connected layer and the result of performing a global average pooling for unit k is $\sum_{x,y} f_{x,y}^k$. The ReLU has been omitted for readability. By generalizing CAM is possible to avoid the model's architectural changes by reinterpreting the Global Average Pooling weighting factors as the backpropagated gradients of any target concept [46]. Then weights of unit k are defined as

$$w_k^c = \frac{1}{n} \sum_x \sum_y \frac{\partial y^c}{\partial A_{x,y}^k} \tag{5}$$

where y^c is the score for class c before the softmax, $A^k_{x,y}$ is the activation at location (x,y) of unit k in the target convolutional layer, and n is the total number of spatial locations in the feature map $(i.e.\ s \times s)$.

Notably, despite the perturbation of the subregions is performed with distinct different techniques, DeepLift [48], $input \times gradient$, and SmoothGrad [52] they all work under a similar setup of $Integrated\ Gradients$ [56] as shown in previous work [8]. For instance, SmoothGrad can be formulated as the $path\ integral$ where the interpolator function samples a single point from a Gaussian distribution $i.e.\ \epsilon_{\sigma} \sim \mathcal{N}\ (\overline{0}, \sigma^2 I)$:

$$\phi_i^{SG}(F^c, x; \mathcal{N}) = \frac{1}{n} \sum_{i=1}^n \left(x + \epsilon_\sigma^i \right) \frac{\partial F^c(x + \epsilon_\sigma^i)}{\partial x}$$
 (6)

3 Method

We first provide some formal definitions. Consider a classification problem where we have a *black-box* model function $f: \mathbb{X} \mapsto \mathbb{Y}$ that maps a set of inputs x from the input space \mathbb{X} to a corresponding set of predictions in the output space \mathbb{Y} such that $x \in \mathbb{X}$ and $\hat{y} \in \mathbb{Y}$ where $x \in \mathbb{R}^D$. The neural network $f_{\theta}: \mathbb{R}^D \to \mathbb{R}^C$ is parameterized by θ with an output space of dimension of C classes where θ are the outcome of the training process *i.e.* producing a mapping $f(x; \theta) = \hat{y}$.

We now define a saliency S as local feature attribution Φ which deterministically map the input vector x to an explanation \hat{e} given some parameters λ :

$$S_{f_{\theta}}: \mathbb{R}^{D} \times \mathbb{F} \times \mathbb{Y} \mapsto \mathbb{R}^{B} = \Phi(\boldsymbol{x}, f, \hat{y}; \lambda) = \hat{e}$$
(7)

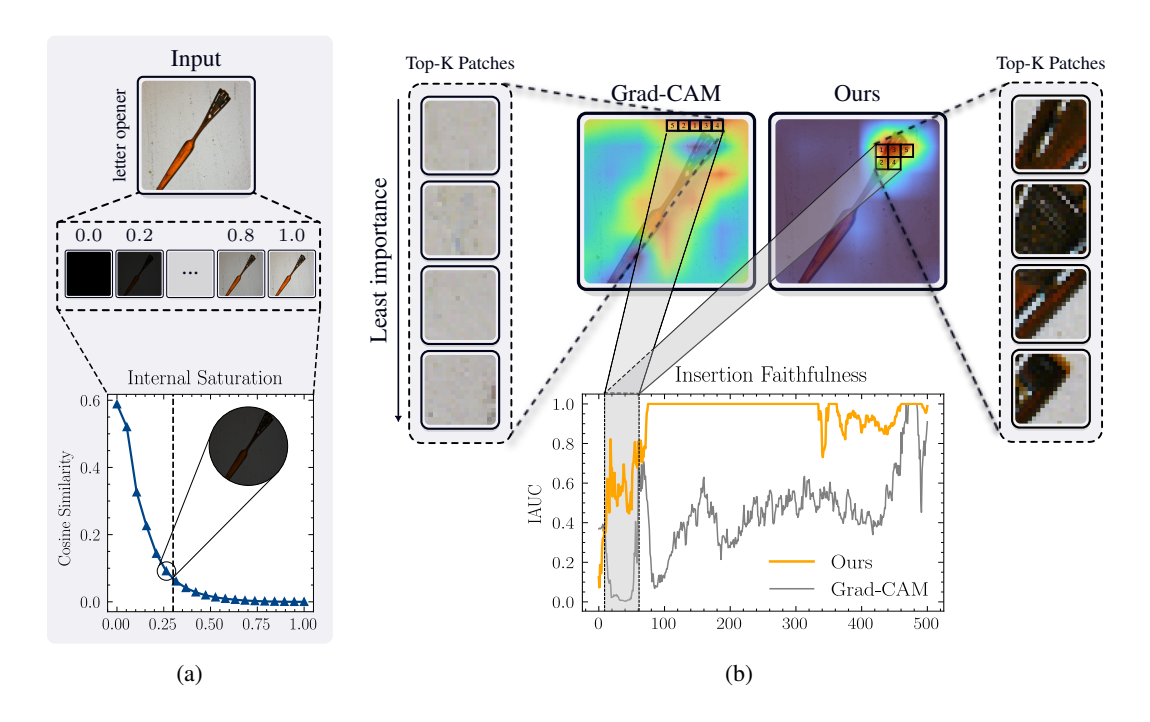


Figure 2: Comparison of attribution maps under internal saturation conditions. Figure 2a illustrates the cosine similarity of the target layer's embeddings with respect to the interpolator parameter (α) (see Appendix B.1 for more details). Figure 2b displays the attribution maps of various methods under saturation conditions. Internal saturation causes the baseline method to under-represent feature importances across saturating ranges. By extracting the top-4 most important features (Figure 2b), it is evident that the baseline method fails to capture relevant discriminative regions, resulting in low insertion AUCs (Figure 2b) as these regions are not deemed important by the model.

The explanation \hat{e} highlights the *discriminative* regions within the input space \mathbb{X} which highly drove the classifier towards \hat{y} . Given the mapping $f(x;\theta) - \hat{y}$, the saliency seeks to encode the influence of the learned behavior modeled by the parameters θ with $\theta_0 \sim p(\theta_0)$, $f_\theta \sim p(\mathbb{D})$ where \mathbb{D} represents the underlying training distribution. Notably, the saliency is computed with an arbitrary dimensionality output shape \mathbb{R}^B which may differ from the input space \mathbb{X} . This holds true for CAM techniques where the output is the products of the subsequent layers up to the target layer l, which often is in a lower dimensionality space due to the applied spatial convolutional blocks. This ultimately involves a transformation T that maps the lower dimensional map back to the original input space \mathbb{X} with $T: \mathbb{R}^B \to \mathbb{R}^D$.

3.1 Reshaping gradient computation

The original formulation of Grad-CAM involves the usage of vanilla gradients, which, by expressing local changes, under-represent feature importances across saturating ranges [55]. Previous works have addressed the saturation phenomena within CAM(s) by implementing popular perturbation techniques [45, 35], however, introducing undesirable side effects *i.e. baseline insensitivity*[54] or poor robustness and stability [6, 56, 21]. Expected Grad-CAM tackles the gradient saturation without interposing insensitivity to its baseline parameter while causally improving four key desiderata in the context of human-interpretable saliencies: (i) fidelity, (ii) robustness, (iii) localization and (iv) complexity. The augmentation operates only on the gradient computation and works under a similar setup as the provably Expected Gradients [18] technique. Let a subset S_k of k features to be perturbed, then an universal, unconstrained scheme that constructs [8] interpolated inputs by replacement [59] can be defined as:

$$\mathbf{x}\left[\mathbf{x}_{S} = x'\right]_{j} = x_{j}\mathbb{I}(j \notin S) + x'\mathbb{I}(j \in S) \tag{8}$$

where \mathbb{I} is the indicator function and x' is a reference baseline. The gradient-scheme which iteratively identifies salient regions in the input space \mathbb{X} , can be extended as the path integral [56] which is

sampled from a reference distribution (Expected Gradients) [18]

$$\Phi_i(f, x; \mathbb{D}) = \int_{x'} \left(\phi_i^{IG}(f, x, x') p_D(x') dx' \right) \tag{9}$$

More generally, we can present an augmentation with a similar scheme which is not bound along a monotonic geometric path, aimed at addressing baseline insensitivity

Definition 3.1. Given a black-box model function f_{θ} and a generic meaningful perturbation I with $I \sim p_D(I)$, where $f_{\theta}^{(l)}$ is the latent representation of f_{θ} at arbitrary layer l. Then any gradient-based CAM scoring mechanism Φ can be formulated as:

$$\Phi(f,x) = \int_{\boldsymbol{I}} f_{\theta}^{(l)}(\boldsymbol{I}\boldsymbol{I}^T) \,\phi^{IG}(f,\mathbf{x},\boldsymbol{I}) \,p_D(\boldsymbol{I}) \,d\boldsymbol{I}$$
(10)

where ϕ^{IG} is any Integrated Gradients attribution framework,

$$\phi^{IG}(f, x, \mathbf{I}) = \int_{\alpha=0}^{1} \nabla f(x + \mathbf{I}(\alpha - 1)) d\alpha$$
 (11)

Remark 3.2. As pointed out by previous work [59] $\Phi(f, x, \mathbf{I})$ can be replaced by any functional kernel which holds the *completeness axiom* [56] *i.e.* $f_{\theta}^{(l)}(\mathbf{I}\mathbf{I}^T) \phi^{IG}(f, x, \mathbf{I}) = f(x) - f(x - \mathbf{I})$ Remark 3.3. If the construction of the perturbation matrix \mathbf{I} occurs over a linear space and using a feature scaling policy over a single constant baseline, then the formula becomes equivalent to Integrated Grad-CAM [45].

Extending this notion, we can formulate a gradient-based local attribution scheme aimed at concurrently improving faithfulness and human-interpretable desirable properties by minimizing infidelity [59]

Definition 3.4. Given the black-box function model $f_{\theta}^{(l)}$ with (l) being any intermediary layer and η any smoothing, distribution-preserving perturbation and I any meaningful perturbation with $\eta \sim \mu_{\eta}$ and $I \sim \mu_{I}$. Then the CAM gradient augmentation can be formulated as:

$$\Phi(f, x, \mathbf{I}) = \left(\int_{\boldsymbol{\eta}} f_{\theta}^{(l)}(\boldsymbol{\eta} \, \boldsymbol{\eta}^T) d\mu_{\boldsymbol{\eta}} \right)^{-1} \int_{\mathbf{I}} f_{\theta}^{(l)}(\mathbf{I} \mathbf{I}^T) \Phi(f, \mathbf{x}, \mathbf{I}) d\mu_{\mathbf{I}}$$
(12)

In this context, the original weighting factors (eq. (5)) can be reformulated as the unaltered linear combination of the smoothed, distribution-sampled, and perturbed integrated gradients²

$$w_k^c = \frac{1}{Z} \sum_i \sum_j \Phi(f_C^{(l)}, x, \mathbf{I}, \boldsymbol{\eta})$$
(13)

3.2 Robust perturbations by data distillation

Recent works have shown that *faithfulness* and *fidelity* are only one of many desirable properties a quality explainer should possess [24]. In this direction, the choice of the perturbation is a key component to (i) preserve the sensitivity axiom [56], (ii) guarantee stability not solely at the input and output, but also w.r.t. to intermediary latent representations [4] and (iii) ensure robustness to infinitesimal perturbations [51, 34]. The usage of constant baselines provides a weak notion of completeness which does not account for noise within the data [59], ultimately showing high sensitivity and high reactivity to noise. Thence, we construct baselines that approximate a given reference distribution rather than a fixed static value with a similar integration scheme as the provably Expected Gradients technique [18]. This allows to maintain a similar gradient smoothing behavior introduced by the usage of a Gaussian kernel [52, 35] but higher robustness as each intermediary sample is distilled with a perturbation I that is close to the underlying training data distribution. Ultimately allowing fewer intermediary samples to fall outside of the data distribution (OOD).

²Note that varying the smoothing distribution alters the type of smoothing kernel applied; when $\eta \sim \mathcal{N}\left(\overline{0}, \sigma^2 I\right)$ then the functional becomes SmoothGrad[52]

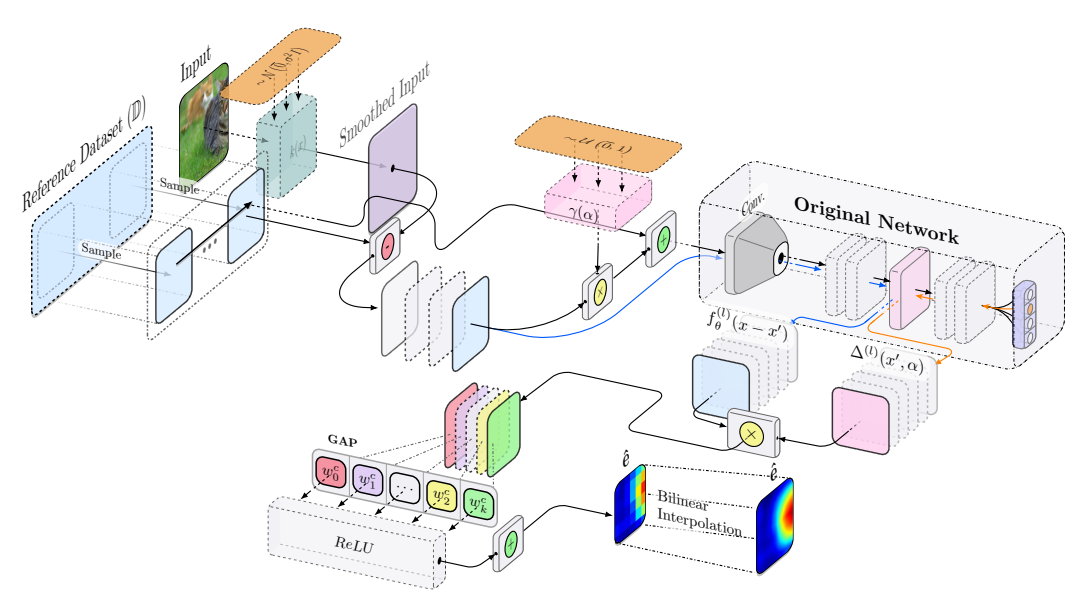


Figure 3: Overview of the proposed Expected Grad-CAM method. Given an input image, a target class, and a reference distribution to sample from, the class-discriminative explanation \hat{e} is computed through input kernel smoothing and difference-from-reference comparisons.

Definition 3.5. Let $\Phi(f, x, I)$ be a local feature attribution scoring method with I a crafted perturbation, and the integral over the outer products of all possible perturbation is inversible $\left(\int II^T d\mu_I\right)^{-1}$. Then the dot product between Φ and I must satisfy the completeness axioms

$$\boldsymbol{I}^{T}\Phi(f,x,\boldsymbol{I}) = f^{c}(x) - f^{c}(x-\boldsymbol{I})$$
(14)

Building on the above definition, we define a robust perturbation derived from the distillation of the underlying data distribution \mathbb{D} using Monte Carlo sampling. The robust perturbation is given by the expectation $\mathbb{E}_{I' \sim \mathbb{D}, \alpha \sim U(0,1)}[I]$, where I = x - I'.

3.3 Expected Grad-CAM and connection to path attribution methods

By thus careful crafting of the perturbation matrix I using a smoothing, distribution-preserving kernel $k(x, \alpha)$ we can formulate Expected Grad-CAM.

Definition 3.6. Let I be a robust data distilling perturbation and η the results of a smoothing kernel with $\mu_I \approx \mathbb{D}$ and $\eta \sim \mu_{\eta}$. Given that ϕ is any Integrated Gradients perturbation scheme, we define the **Expected Grad-CAM** weights of unit k as:

$$w_k^c = \frac{1}{n} \sum_{i,j} \mathbb{E}_{I' \sim \mu_I} \left[k(x) \int_{I} f_{\theta}^{(l)}(II^T) \phi(f, \boldsymbol{x}, I) d\mu_I \right]$$
(15)

where,

$$k(x) = \left(\int_{\boldsymbol{\eta}} f_{\theta}^{(l)}(\boldsymbol{\eta} \, \boldsymbol{\eta}^T) \, d\mu_{\boldsymbol{\eta}} \right)^{-1} \tag{16}$$

Thus k(x) is the first moment of all the smoothing functionals under the distribution μ_{η} encoded at an arbitrary intermediary layer (l) and (i,j) the feature map spatial locations. Explicitly, $f_{\theta}^{(l)}$ produces layer-specific latent representations modeled under the learned behavior θ . The smoothing kernel k(x) directly controls the sensitivity of the explanation around the sample x, implicitly driving the complexity of the explanation. Whereas any smoothing kernel can be adopted, we found that $\mu_{\eta} \sim \mathcal{N}\left(\overline{0}, \sigma^2 \mathbf{I}\right)$ and $\mu_{\eta} \sim \mathcal{U}(0,1)$ produces similar smoothing performances, therefore the latter has been used in the experiments.

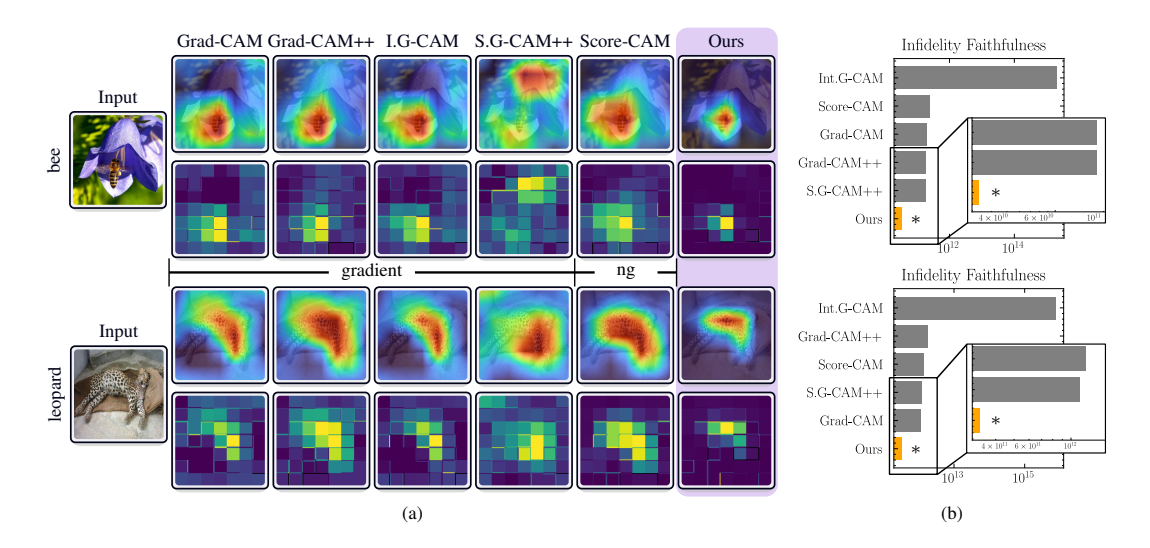


Figure 4: Comparison of saliencies generated by different gradient- and non-gradient-based methods. Figure 4a shows the superimposed (top row) and raw coarse saliencies (bottom row) generated by each method. Figure 4b presents the Infidelity scores [59] (using log-scale) for the different methods. While baseline methods are noisy with low localization, our method produces sharper, more localized explanations, outperforming even non-gradient-based techniques, and resulting in significantly lower infidelity scores (fig. 4b).

Definition 3.7. Let ξ be any matrix perturbation with $\xi \sim \mu_{\xi}$ and $\xi \xi^T$ produce a covariance matrix such that $\xi \xi^T = K_{\xi \xi}$. Then $\int \xi p(\xi) d\xi$ corresponds to the expectation of the perturbation ξ under that distribution.

$$\mathbb{E}[\xi] = \int \xi \mu_{\xi}(\xi) \ d\xi \tag{17}$$

Definition 3.8. Let $S_{f_{\theta}}^{C}$ the coarse saliency generated for the model f_{θ} upon class C and $A^{k,(l)}$ the activations k of an arbitrary layer l. Then the explanation $S_{f_{\theta}}^{C}$ is constructed as the unaltered linear combination of the smoothed perturbed expected gradients as follows:

$$S_{f_{\theta}}^{C} = \text{ReLU}\left(\sum_{k}^{N} w_{k}^{c} A^{k,(l)}\right)$$
(18)

As discussed by previous work [8] and introduced at the beginning of this paper, despite the perturbations are crafted with different distinct techniques and thus are more consequential and insightful to discuss unconstrained non-monotonic perturbations, such schemes can always be re-formulated under a geometrical path integral method setup. That is, given the universal formula for a path method [56] $\phi_i^{\gamma}(f,x)$ and its interpolator function γ as:

$$\phi_i^{\gamma}(f, x) = \int_{\alpha=0}^1 \frac{\partial F(\gamma(\alpha))}{\partial \gamma_i(\alpha)} \frac{\partial \gamma_i(\alpha)}{\partial \alpha} d\alpha \qquad \text{where} \qquad \begin{array}{c} \gamma(0) := x', \\ \gamma(1) := x \end{array}$$
 (19)

Given a linear interpolation path such that the one employed in IG [56]:

$$\gamma^{IG}(\alpha) = x' + \alpha \times (x - x')$$
 where $\alpha \in [0, 1]$ (20)

Definition 3.9. Let $y_{\gamma(\alpha)}^c$ the class-specific model's output at the interpolated point α given the interpolator function γ . Then the linear Path Integral formulation of the **Expected Grad-CAM**

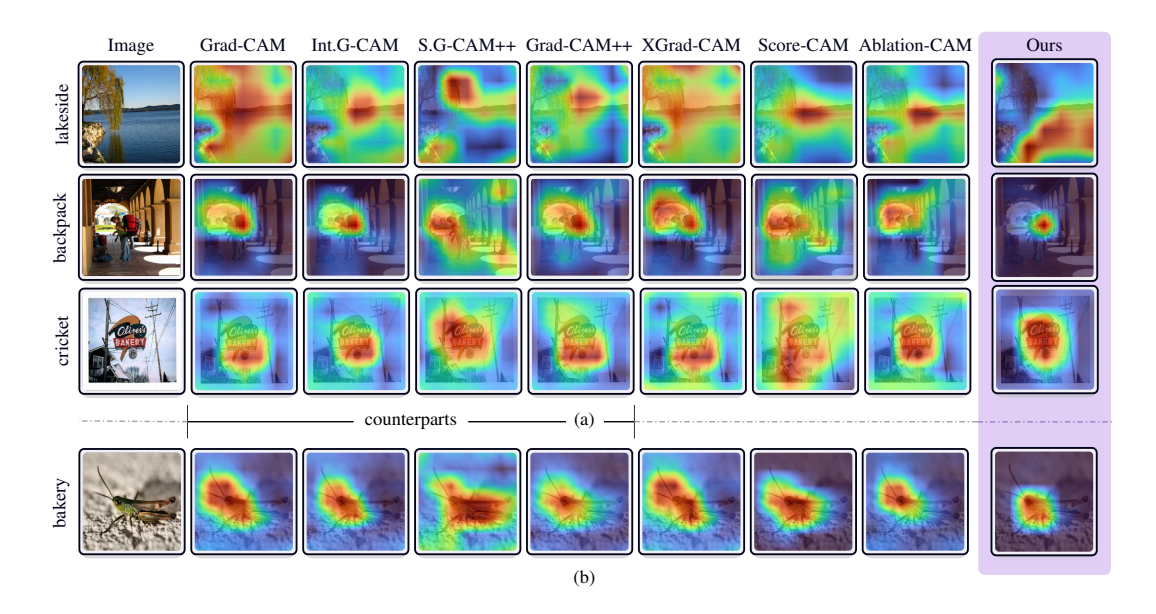


Figure 5: Comparison of attribution maps for various methods under normal conditions (5b) and internal saturation conditions (5a). Our method (*Expected Grad-CAM*) provides sharper, more localized, and more stable explanations compared to its direct counterparts, namely *Grad-CAM* [46], *Grad-CAM*++ [13], *Smooth Grad-CAM*++ [35], and *Integrated Grad-CAM* [45]. Additionally, it offers competitive explanations compared to non-gradient and more complex methods through gradient augmentation. For a complete comparison, refer to Appendix C.

weights at spatial location (i, j) can be denoted as:

$$w_{k}^{c} = \underset{x' \sim \mathbf{D}, \alpha \sim U(0,1)}{\mathbb{E}} \left[k(x,\alpha) \frac{\partial y_{\gamma(\alpha)}^{c}}{\partial A_{i,j}^{k,(l)}} \frac{\partial \gamma(\alpha)}{\partial \alpha} \right]$$

$$= \underset{x' \sim \mathbf{D}, \alpha \sim U(0,1)}{\mathbb{E}} \left[k(x,\alpha) \left[f_{\theta}^{(l)} \left(x_{i,j} - x_{i,j}' \right) \Delta_{i,j}^{k,(l)} (x',\alpha) \right] \right]$$

$$= \frac{1}{n} \sum_{s=1}^{n} k(x,\alpha) \left[f_{\theta}^{(l)} \left(x_{i,j} - x_{i,j}', x_{i,j}' \right) \Delta_{i,j}^{k,(l)} (x',x_{i,j},x_{i,j}', x_{i,j}') \right]$$
(21)

where,

$$\Delta_{i,j}^{k,(l)}(x',\alpha) = \frac{\partial f_{\theta}^{c}\left(x' + \alpha\left(x - x'\right)\right)}{\partial A_{i,j}^{k,(l)}}$$
(22)

represents the partial derivative of the class c output with respect to the activation $A_{i,j}^{k,(l)}$, evaluated at the interpolated point $x' + \alpha(x - x')$ for a baseline x' sampled from a distribution D.

4 Experiments

In line with previous works [27, 58, 27] we evaluate our proposed method quantitatively and qualitatively.

Datasets. We consider the *ILSVRC2012* [42], *CIFAR10* [26] and *COCO* [32] with images of size 224×224 . The first two datasets have been used across the quantitative metrics, while the latter only for the localization evaluations, where the segmentation masks of each sample have been employed. **Models.** Each metric is evaluated across popular feed-forward CNN architecture. In style with prior literature, we restricted our analysis to *VGG16* [49], *ResNet50* [23] and *AlexNet* [31]. In all cases, the default pre-trained *PyTorch* torchvision implementation has been adopted.

Metrics. In contrast to prior works, we comprehensively evaluate our technique across an extensive set of traditional and modern metrics. We provide a full characterization of the behavior of our

Table 1: Faithfulness, Robustness and Complexity Metrics. Values evaluated on ILSVRC2012[42] on VGG16 [49]. Extended results are available in Appendix B.

	I	aithfulnes	SS		Robustness	Comp		lexity
Method	↓ P.F.	↑ Suff.	↓ Inf.	↓ L. Est.	↓ M. Sens.	↓ A. Sens.	↓ CP.	↑ SP.
Grad-CAM	55.36	1.91	8.12	0.38	0.27	0.20	10.56	0.38
Grad-CAM++	56.93	1.87	7.98	0.32	0.192	0.15	10.53	0.40
Sm. Grad-CAM++	56.38	1.89	7.50	0.51	0.51	0.27	10.60	0.35
Int. Grad-CAM	57.36	1.83	8.92	1.05	1.00	1.00	10.59	0.36
HiRes-CAM	57.49	1.74	5.73	0.99	1.00	1.00	10.54	0.40
XGrad-CAM	57.32	1.98	7.88	0.37	0.23	0.18	10.56	0.38
LayerCAM	58.15	1.74	7.22	0.31	0.19	0.14	10.56	0.38
Score-CAM	5.37	1.91	7.39	$\overline{0.68}$	0.65	0.53	10.56	0.38
Ablation-CAM	57.36	1.83	7.28	1.05	1.00	1.00	10.59	0.36
Expected Grad-CAM	62.39	2.10	4.99	0.24	0.194	<u>0.15</u>	10.43	0.47

method by evaluating not just faithfulness, but rather all the different explanatory qualities across recent explanation quality grouping [24] *i.e.* (i) Faithfulness, (ii) Robustness, (iii) Complexity, and (iv) Localization. In Table 2 are presented all the evaluated metrics categorized by quality groupings, while the extended quantitative results are available in Appendix B.

Baselines. We compare our proposed technique against recent and relevant methods including Grad-CAM [46], Grad-CAM++ [13], Smooth Grad-CAM++ [35], Integrated Grad-CAM [45], HiRes-CAM [16], XGrad-CAM [20], LayerCAM [27], Score-CAM [58] and Ablation-CAM [15]

Qualitative evaluations In Figure 5 we present an excerpt of the explanations generated during the computation of the quantitative evaluations on the *ILSVRC2012* validation set. By inspecting the attribution sparsity and localization characteristics of each explanation, our method (*Expected Grad-CAM*), generally produces saliencies that are more localized and focused on the attuned human-centric understanding of the composition of the attributes of the labels. An explanation designed for human fruition *i.e.* aimed at building the model's trustworthiness should be encoded as such to not *disrupt trust*; this implies that an *human-interpretable* explanation should be restricted to the most important pertinent and stable features: it should contains the least number of stable features which do maximally fulfill the notion of fidelity (figs. 4 and 6). In Figure 5a it is observed qualitatively that every other compared attribution method breaks such condition: given the labels *lakeside* and *backpack* the explanations highlights areas which are not pertinent with label-related attributes *i.e.* the sky and portions of the tree (fig. 5a) and parts of the background (fig. 5b) respectively.

Quantitative evaluations Following, we assess the validity of our claims quantitatively across various desirable explanatory qualities. The extended quantitative results are available in Appendix B.

Faithfulness. Examining traditional *faithfulness* metrics (Insertion and Deletion AUCs) across popular benchmarking networks on a large chunk of *ILSVRC2012*, showed promising results (table 3). Our method *Expected Grad-CAM*, outperformed jointly its gradient and non-gradient-based counterparts as well as more advanced variation of CAM, which do not solely rely on a gradient augmentation, in both the *insertion* and *deletion* aspects. Towards a more comprehensive comparison, we then verified our technique against more recent metrics. Unsurprisingly, *IROF* [40] and *Pixel Flipping* [10] (table 1) showed agreement with traditional metrics as they fundamentally assess similar explanatory qualities. Our technique scored higher than others on the *Sufficiency* [14] metric, due to greater *stability* and *robustness* (table 1). Finally, we tested *Expected Grad-CAM*'s performances in terms of *infidelity* [59], which, expectedly showed the highest results. For fairness, we provided also results with respect to known metrics that produce disagreeing rank-order results [41, 24, 25] *i.e. Faithfulness Estimate* [7] where our approach was the second best scoring explainer.

Stability. In table 6 are presented the results w.r.t. to the relative- input and out stability metrics. our method showed the lowest score overall (*highest stability*), while achieving best or second-best robustness scores (table 1).

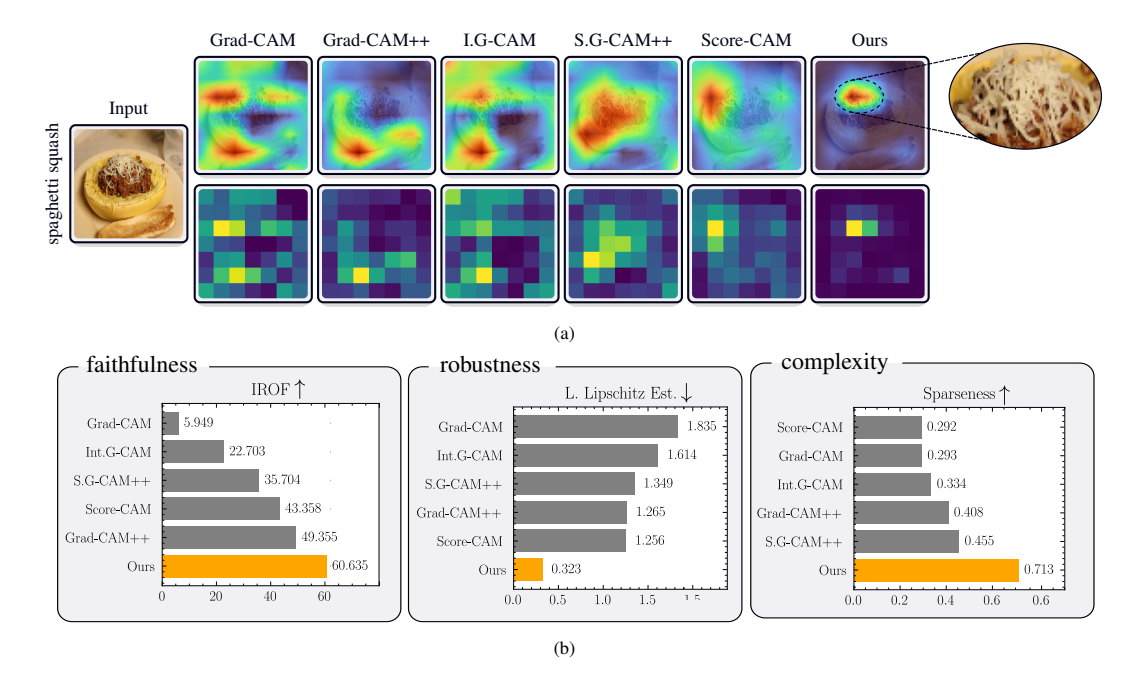


Figure 6: Comparison of saliencies generated by different gradient- and non-gradient-based methods. Figure 6a shows the superimposed (top row) and raw coarse saliencies (bottom row) generated by each method. Our method consistently produces more focused and sharper saliencies compared to both gradient-based and non-gradient-based methods (e.g., Score-CAM). Figure 6b demonstrates that our approach concurrently improves key xAI properties: (i) faithfulness, (ii) robustness, and (iii) complexity, significantly outperforming even non-gradient-based methods.

5 Conclusion and broader impact

In this paper, we advanced current CAM's gradient faithfulness by proposing *Expected Grad-CAM* which simultaneously addresses the saturation and sensitivity phenomena, without introducing undesirable side effects. Revisiting the original formulation as the smoothed expectation of the perturbed integrated gradients, one can concurrently construct more faithful, localized, and robust explanations that minimize infidelity. Despite qualitative assessment being highly subjective, quantitative evaluations are also teeming with indeterminate, ambiguous results that span further than the rank-order issues. While faithfulness is a universally desirable underlying explanatory quality, individual metrics, which do assess such property, only define a distinct notion of such a multifaceted trait, potentially delineating unwanted aspects. While careful modulation of the smoothing functional allows for fine-grained control of the complexity characteristic of the explanation, where, through sensitivity reduction, produces more human-interpretable saliencies; it contrastingly influences the current notions of faithfulness. Perhaps, further adaption of existing metrics may be necessary to embody human-interpretability; nevertheless, existing qualitative and quantitative assessments proved the superiority of our approach.

Broader impact. This paper highlights the value and effectiveness of Expected Grad-CAM in comparison to current state-of-the-art approaches across a comprehensive set of modern evaluation metrics. We demonstrated that our technique satisfies many desirable xAI properties by producing explanations that are highly concentrated on the least number of stable robust, features. Our experiments revealed that many state-of-the-art approaches underperform on modern metrics. Ultimately, as our technique is intended to replace the original formulation of Grad-CAM, we hope new and existing approaches will build on it.

References

- [1] Kumar Abhishek and Deeksha Kamath. Attribution-based XAI Methods in Computer Vision: A Review. 11 2022. doi: 10.48550/arxiv.2211.14736. URL https://arxiv.org/abs/2211.14736v1.
- [2] Amina Adadi and Mohammed Berrada. Peeking Inside the Black-Box: A Survey on Explainable Artificial Intelligence (XAI). *IEEE Access*, 6:52138–52160, 9 2018. ISSN 21693536. doi: 10.1109/ACCESS.2018.2870052.
- [3] Julius Adebayo, Justin Gilmer, Ian Goodfellow, and Been Kim. Local Explanation Methods for Deep Neural Networks Lack Sensitivity to Parameter Values. 6th International Conference on Learning Representations, ICLR 2018 Workshop Track Proceedings, 10 2018. URL https://arxiv.org/abs/1810.03307v1.
- [4] Chirag Agarwal, Nari Johnson, Martin Pawelczyk, Satyapriya Krishna, Eshika Saxena, Marinka Zitnik, and Himabindu Lakkaraju. Rethinking Stability for Attribution-based Explanations. 3 2022. URL https://arxiv.org/abs/2203.06877v1.
- [5] Kamran Alipour, Aditya Lahiri, Ehsan Adeli, Babak Salimi, and Michael Pazzani. Explaining Image Classifiers Using Contrastive Counterfactuals in Generative Latent Spaces. 6 2022. URL https://arxiv.org/abs/2206.05257v1.
- [6] David Alvarez-Melis and Tommi S. Jaakkola. On the Robustness of Interpretability Methods. 6 2018. URL https://arxiv.org/abs/1806.08049v1.
- [7] David Alvarez-Melis and Tommi S. Jaakkola. Towards Robust Interpretability with Self-Explaining Neural Networks. Advances in Neural Information Processing Systems, 2018-December:7775–7784, 6 2018. ISSN 10495258. URL https://arxiv.org/abs/1806.07538v2.
- [8] Marco Ancona, Enea Ceolini, Cengiz Öztireli, and Markus Gross. Towards better understanding of gradient-based attribution methods for Deep Neural Networks. *6th International Conference on Learning Representations, ICLR 2018 Conference Track Proceedings*, 11 2017. URL https://arxiv.org/abs/1711.06104v4.
- [9] Leila Arras, Ahmed Osman, and Wojciech Samek. Ground Truth Evaluation of Neural Network Explanations with CLEVR-XAI. *Information Fusion*, 81:14–40, 3 2020. doi: 10.1016/j.inffus. 2021.11.008. URL http://arxiv.org/abs/2003.07258http://dx.doi.org/10.1016/j.inffus.2021.11.008.
- [10] Sebastian Bach, Alexander Binder, Grégoire Montavon, Frederick Klauschen, Klaus Robert Müller, and Wojciech Samek. On Pixel-Wise Explanations for Non-Linear Classifier Decisions by Layer-Wise Relevance Propagation. *PLoS ONE*, 10 (7), 7 2015. ISSN 19326203. doi: 10.1371/JOURNAL.PONE.0130140. URL /pmc/articles/PMC4498753//pmc/articles/PMC4498753/?report=abstracthttps://www.ncbi.nlm.nih.gov/pmc/articles/PMC4498753/.
- [11] Umang Bhatt, Adrian Weller, and José M.F. Moura. Evaluating and Aggregating Feature-based Model Explanations. *IJCAI International Joint Conference on Artificial Intelligence*, 2021-January:3016–3022, 5 2020. ISSN 10450823. doi: 10.24963/ijcai.2020/417. URL https://arxiv.org/abs/2005.00631v1.
- [12] Prasad Chalasani, Jiefeng Chen, Amrita Roy Chowdhury, Somesh Jha, and Xi Wu. Concise Explanations of Neural Networks using Adversarial Training. 37th International Conference on Machine Learning, ICML 2020, PartF168147-2:1360–1368, 10 2018. URL https://arxiv.org/abs/1810.06583v9.
- [13] Aditya Chattopadhay, Anirban Sarkar, Prantik Howlader, and Vineeth N. Balasubramanian. Grad-CAM++: Improved Visual Explanations for Deep Convolutional Networks. *Proceedings 2018 IEEE Winter Conference on Applications of Computer Vision, WACV 2018*, 2018-January: 839–847, 10 2017. doi: 10.1109/wacv.2018.00097. URL https://arxiv.org/abs/1710. 11063v3.

- [14] Sanjoy Dasgupta, Nave Frost, and Michal Moshkovitz. Framework for Evaluating Faithfulness of Local Explanations. *Proceedings of Machine Learning Research*, 162:4794–4815, 2 2022. ISSN 26403498. URL https://arxiv.org/abs/2202.00734v1.
- [15] Saurabh Desai and Harish G. Ramaswamy. Ablation-CAM: Visual explanations for deep convolutional network via gradient-free localization. *Proceedings - 2020 IEEE Winter Con*ference on Applications of Computer Vision, WACV 2020, pages 972–980, 3 2020. doi: 10.1109/WACV45572.2020.9093360.
- [16] Rachel Lea Draelos and Lawrence Carin. Use HiResCAM instead of Grad-CAM for faithful explanations of convolutional neural networks. 11 2020. URL https://arxiv.org/abs/ 2011.08891v4.
- [17] Alexandre Englebert, Olivier Cornu, and Christophe De Vleeschouwer. Poly-CAM: High resolution class activation map for convolutional neural networks. 4 2022. URL https://arxiv.org/abs/2204.13359v2.
- [18] Gabriel Erion, Joseph D. Janizek, Pascal Sturmfels, Scott M. Lundberg, and Su In Lee. Improving performance of deep learning models with axiomatic attribution priors and expected gradients. *Nature Machine Intelligence*, 3(7):620–631, 6 2019. ISSN 25225839. doi: 10.48550/arxiv.1906.10670. URL https://arxiv.org/abs/1906.10670v2.
- [19] Ruth Fong and Andrea Vedaldi. Interpretable Explanations of Black Boxes by Meaningful Perturbation. *Proceedings of the IEEE International Conference on Computer Vision*, 2017-October:3449–3457, 4 2017. doi: 10.1109/ICCV.2017.371. URL http://arxiv.org/abs/1704.03296http://dx.doi.org/10.1109/ICCV.2017.371.
- [20] Ruigang Fu, Qingyong Hu, Xiaohu Dong, Yulan Guo, Yinghui Gao, and Biao Li. Axiombased Grad-CAM: Towards Accurate Visualization and Explanation of CNNs. 8 2020. URL https://arxiv.org/abs/2008.02312v4.
- [21] Amirata Ghorbani, Abubakar Abid, and James Zou. Interpretation of Neural Networks is Fragile. 33rd AAAI Conference on Artificial Intelligence, AAAI 2019, 31st Innovative Applications of Artificial Intelligence Conference, IAAI 2019 and the 9th AAAI Symposium on Educational Advances in Artificial Intelligence, EAAI 2019, pages 3681–3688, 10 2017. ISSN 2159-5399. doi: 10.1609/aaai.v33i01.33013681. URL https://arxiv.org/abs/1710.10547v2.
- [22] Leilani H. Gilpin, David Bau, Ben Z. Yuan, Ayesha Bajwa, Michael Specter, and Lalana Kagal. Explaining Explanations: An Overview of Interpretability of Machine Learning. 2018 IEEE 5th International Conference on Data Science and Advanced Analytics (DSAA), pages 80–89, 1 2018. doi: 10.1109/DSAA.2018.00018.
- [23] Kaiming He, Xiangyu Zhang, Shaoqing Ren, and Jian Sun. Deep Residual Learning for Image Recognition. *Proceedings of the IEEE Computer Society Conference on Computer Vision and Pattern Recognition*, 2016-December:770–778, 12 2015. ISSN 10636919. doi: 10.1109/CVPR.2016.90. URL https://arxiv.org/abs/1512.03385v1.
- [24] Anna Hedström, tu-berlinde Leander Weber, Dilyara Bareeva, Daniel Krakowczyk, Franz Motzkus, Wojciech Samek, Sebastian Lapuschkin, and Marina M-C Höhne. Quantus: An Explainable AI Toolkit for Responsible Evaluation of Neural Network Explanations and Beyond. *Journal of Machine Learning Research*, 24:1–11, 2 2022. URL https://arxiv.org/abs/2202.06861v3.
- [25] Anna Hedström, Philine Bommer, Kristoffer K. Wickstrøm, Wojciech Samek, Sebastian Lapuschkin, and Marina M. C. Höhne. The Meta-Evaluation Problem in Explainable AI: Identifying Reliable Estimators with MetaQuantus. 2 2023. URL https://arxiv.org/abs/2302.07265v2.
- [26] Tien Ho-Phuoc. CIFAR10 to Compare Visual Recognition Performance between Deep Neural Networks and Humans. 11 2018. URL https://arxiv.org/abs/1811.07270v2.
- [27] Peng Tao Jiang, Chang Bin Zhang, Qibin Hou, Ming Ming Cheng, and Yunchao Wei. LayerCAM: Exploring hierarchical class activation maps for localization. *IEEE Transactions on Image Processing*, 30:5875–5888, 2021. ISSN 19410042. doi: 10.1109/TIP.2021.3089943.

- [28] Beomsu Kim, Junghoon Seo, Seunghyeon Jeon, Jamyoung Koo, Jeongyeol Choe, and Taegyun Jeon. Why are Saliency Maps Noisy? Cause of and Solution to Noisy Saliency Maps. Proceedings 2019 International Conference on Computer Vision Workshop, IC-CVW 2019, pages 4149–4157, 2 2019. doi: 10.1109/ICCVW.2019.00510. URL https://arxiv.org/abs/1902.04893v3.
- [29] Pieter Jan Kindermans, Sara Hooker, Julius Adebayo, Maximilian Alber, Kristof T. Schütt, Sven Dähne, Dumitru Erhan, and Been Kim. The (Un)reliability of saliency methods. Lecture Notes in Computer Science (including subseries Lecture Notes in Artificial Intelligence and Lecture Notes in Bioinformatics), 11700 LNCS:267–280, 11 2017. ISSN 16113349. doi: 10.48550/arxiv.1711.00867. URL https://arxiv.org/abs/1711.00867v1.
- [30] Maximilian Kohlbrenner, Alexander Bauer, Shinichi Nakajima, Alexander Binder, Wojciech Samek, and Sebastian Lapuschkin. Towards Best Practice in Explaining Neural Network Decisions with LRP. Proceedings of the International Joint Conference on Neural Networks, 10 2019. doi: 10.1109/IJCNN48605.2020.9206975. URL https://arxiv.org/abs/1910.09840v3.
- [31] Alex Krizhevsky, Ilya Sutskever, and Geoffrey E. Hinton. ImageNet Classification with Deep Convolutional Neural Networks. *Advances in Neural Information Processing Systems*, 25, 2012. URL http://code.google.com/p/cuda-convnet/.
- [32] Tsung Yi Lin, Michael Maire, Serge Belongie, James Hays, Pietro Perona, Deva Ramanan, Piotr Dollár, and C. Lawrence Zitnick. Microsoft COCO: Common Objects in Context. Lecture Notes in Computer Science (including subseries Lecture Notes in Artificial Intelligence and Lecture Notes in Bioinformatics), 8693 LNCS(PART 5):740–755, 5 2014. ISSN 16113349. doi: 10.1007/978-3-319-10602-1{_}48. URL https://arxiv.org/abs/1405.0312v3.
- [33] Zachary C. Lipton. The Mythos of Model Interpretability. Communications of the ACM, 61 (10):35-43, 6 2016. ISSN 15577317. doi: 10.1145/3233231. URL https://arxiv.org/abs/1606.03490v3.
- [34] Seyed-Mohsen Moosavi-Dezfooli, Alhussein Fawzi, Omar Fawzi, and Pascal Frossard. Universal adversarial perturbations. URL https://github.com/.
- [35] Daniel Omeiza, Skyler Speakman, Celia Cintas, and Komminist Weldermariam. Smooth Grad-CAM++: An Enhanced Inference Level Visualization Technique for Deep Convolutional Neural Network Models. *CoRR*, abs/1908.01224, 8 2019. doi: 10.48550/arxiv.1908.01224. URL https://arxiv.org/abs/1908.01224v1.
- [36] Vitali Petsiuk, Abir Das, and Kate Saenko. RISE: Randomized Input Sampling for Explanation of Black-box Models. *British Machine Vision Conference 2018*, *BMVC 2018*, 6 2018. URL https://arxiv.org/abs/1806.07421v3.
- [37] Changqing Qiu, Fusheng Jin, and Yining Zhang. Fine-Grained and High-Faithfulness Explanations for Convolutional Neural Networks. 3 2023. URL https://arxiv.org/abs/2303.09171v1.
- [38] Anna Rakitianskaia and Andries Engelbrecht. Measuring saturation in neural networks. *Proceedings 2015 IEEE Symposium Series on Computational Intelligence, SSCI 2015*, pages 1423–1430, 2015. doi: 10.1109/SSCI.2015.202.
- [39] Marco Tulio Ribeiro, Sameer Singh, and Carlos Guestrin. "Why Should I Trust You?": Explaining the Predictions of Any Classifier. NAACL-HLT 2016 2016 Conference of the North American Chapter of the Association for Computational Linguistics: Human Language Technologies, Proceedings of the Demonstrations Session, pages 97–101, 2 2016. doi: 10.18653/v1/n16-3020. URL https://arxiv.org/abs/1602.04938v3.
- [40] Laura Rieger and Lars Kai Hansen. IROF: a low resource evaluation metric for explanation methods. 3 2020. URL https://arxiv.org/abs/2003.08747v1.

- [41] Yao Rong, Tobias Leemann, Vadim Borisov, Gjergji Kasneci, and Enkelejda Kasneci. A Consistent and Efficient Evaluation Strategy for Attribution Methods. *Proceedings of Machine Learning Research*, 162:18770–18795, 2 2022. ISSN 26403498. URL https://arxiv.org/abs/2202.00449v2.
- [42] Olga Russakovsky, Jia Deng, Hao Su, Jonathan Krause, Sanjeev Satheesh, Sean Ma, Zhiheng Huang, Andrej Karpathy, Aditya Khosla, Michael Bernstein, Alexander C Berg, Li Fei-Fei, O Russakovsky, J Deng, H Su, J Krause, S Satheesh, S Ma, Z Huang, A Karpathy, A Khosla, M Bernstein, A C Berg, and L Fei-Fei. ImageNet Large Scale Visual Recognition Challenge. *International Journal of Computer Vision*, 115(3):211–252, 9 2014. ISSN 15731405. doi: 10.1007/s11263-015-0816-y. URL https://arxiv.org/abs/1409.0575v3.
- [43] Wojciech Samek, Thomas Wiegand, and Klaus-Robert Müller. Explainable Artificial Intelligence: Understanding, Visualizing and Interpreting Deep Learning Models. *CoRR*, abs/1708.08296, 8 2017. doi: 10.48550/arxiv.1708.08296. URL https://arxiv.org/abs/1708.08296v1.
- [44] Wojciech Samek, Grégoire Montavon, Sebastian Lapuschkin, Christopher J. Anders, and Klaus Robert Müller. Explaining Deep Neural Networks and Beyond: A Review of Methods and Applications. *Proceedings of the IEEE*, 109(3):247–278, 3 2021. ISSN 15582256. doi: 10.1109/JPROC.2021.3060483.
- [45] Sam Sattarzadeh, Mahesh Sudhakar, Konstantinos N. Plataniotis, Jongseong Jang, Yeonjeong Jeong, and Hyunwoo Kim. Integrated Grad-CAM: Sensitivity-Aware Visual Explanation of Deep Convolutional Networks via Integrated Gradient-Based Scoring. ICASSP, IEEE International Conference on Acoustics, Speech and Signal Processing Proceedings, 2021-June:1775–1779, 2 2021. ISSN 15206149. doi: 10.1109/ICASSP39728.2021.9415064. URL https://arxiv.org/abs/2102.07805v1.
- [46] Ramprasaath R. Selvaraju, Michael Cogswell, Abhishek Das, Ramakrishna Vedantam, Devi Parikh, and Dhruv Batra. Grad-CAM: Visual Explanations from Deep Networks via Gradient-based Localization. *International Journal of Computer Vision*, 128(2):336–359, 10 2016. doi: 10.1007/s11263-019-01228-7. URL http://arxiv.org/abs/1610.02391http://dx.doi.org/10.1007/s11263-019-01228-7.
- [47] Xiangwei Shi, Seyran Khademi, Yunqiang Li, and Jan van Gemert. Zoom-CAM: Generating Fine-grained Pixel Annotations from Image Labels. *Proceedings International Conference on Pattern Recognition*, pages 10289–10296, 10 2020. ISSN 10514651. doi: 10.1109/ICPR48806. 2021.9412980. URL https://arxiv.org/abs/2010.08644v1.
- [48] Avanti Shrikumar, Peyton Greenside, and Anshul Kundaje. Learning Important Features Through Propagating Activation Differences. *34th International Conference on Machine Learning, ICML* 2017, 7:4844–4866, 4 2017. URL https://arxiv.org/abs/1704.02685v2.
- [49] Karen Simonyan and Andrew Zisserman. Very Deep Convolutional Networks for Large-Scale Image Recognition. 3rd International Conference on Learning Representations, ICLR 2015 Conference Track Proceedings, 9 2014. URL https://arxiv.org/abs/1409.1556v6.
- [50] Karen Simonyan, Andrea Vedaldi, and Andrew Zisserman. Deep Inside Convolutional Networks: Visualising Image Classification Models and Saliency Maps. 2nd International Conference on Learning Representations, ICLR 2014 - Workshop Track Proceedings, 12 2013. doi: 10.48550/ arxiv.1312.6034. URL https://arxiv.org/abs/1312.6034v2.
- [51] Dylan Slack, Sophie Hilgard, Emily Jia, Sameer Singh, and Himabindu Lakkaraju. Fooling LIME and SHAP: Adversarial Attacks on Post hoc Explanation Methods. *AIES 2020 Proceedings of the AAAI/ACM Conference on AI, Ethics, and Society*, pages 180–186, 11 2019. doi: 10.1145/3375627.3375830. URL https://arxiv.org/abs/1911.02508v2.
- [52] Daniel Smilkov, Nikhil Thorat, Been Kim, Fernanda Viégas, and Martin Wattenberg. Smooth-Grad: removing noise by adding noise. *CoRR*, abs/1706.03825, 6 2017. doi: 10.48550/arxiv. 1706.03825. URL https://arxiv.org/abs/1706.03825v1.

- [53] Jost Tobias Springenberg, Alexey Dosovitskiy, Thomas Brox, and Martin Riedmiller. Striving for Simplicity: The All Convolutional Net. 3rd International Conference on Learning Representations, ICLR 2015 Workshop Track Proceedings, 12 2014. URL https://arxiv.org/abs/1412.6806v3.
- [54] Mukund Sundararajan and Ankur Taly. A Note about: Local Explanation Methods for Deep Neural Networks lack Sensitivity to Parameter Values. 6 2018. URL https://arxiv.org/ abs/1806.04205v1.
- [55] Mukund Sundararajan, Ankur Taly, and Qiqi Yan. Gradients of Counterfactuals. 11 2016. URL https://arxiv.org/abs/1611.02639v2.
- [56] Mukund Sundararajan, Ankur Taly, and Qiqi Yan. Axiomatic Attribution for Deep Networks. 34th International Conference on Machine Learning, ICML 2017, 7:5109–5118, 3 2017. doi: 10.48550/arxiv.1703.01365. URL https://arxiv.org/abs/1703.01365v2.
- [57] Jonas Theiner, Eric Muller-Budack, and Ralph Ewerth. Interpretable Semantic Photo Geolocation. *Proceedings 2022 IEEE/CVF Winter Conference on Applications of Computer Vision, WACV 2022*, pages 1474–1484, 4 2021. doi: 10.1109/WACV51458.2022.00154. URL https://arxiv.org/abs/2104.14995v2.
- [58] Haofan Wang, Zifan Wang, Mengnan Du, Fan Yang, Zijian Zhang, Sirui Ding, Piotr Mardziel, and Xia Hu. Score-CAM: Score-Weighted Visual Explanations for Convolutional Neural Networks. *IEEE Computer Society Conference on Computer Vision and Pattern Recognition Workshops*, 2020-June:111–119, 10 2019. ISSN 21607516. doi: 10.1109/CVPRW50498.2020. 00020. URL https://arxiv.org/abs/1910.01279v2.
- [59] Chih Kuan Yeh, Cheng Yu Hsieh, Arun Sai Suggala, David I. Inouye, and Pradeep Ravikumar. On the (In)fidelity and Sensitivity for Explanations. Advances in Neural Information Processing Systems, 32, 1 2019. ISSN 10495258. doi: 10.48550/arxiv.1901.09392. URL https://arxiv.org/abs/1901.09392v4.
- [60] Matthew D. Zeiler and Rob Fergus. Visualizing and Understanding Convolutional Networks. Lecture Notes in Computer Science (including subseries Lecture Notes in Artificial Intelligence and Lecture Notes in Bioinformatics), 8689 LNCS(PART 1):818–833, 11 2013. ISSN 16113349. doi: 10.48550/arxiv.1311.2901. URL https://arxiv.org/abs/1311.2901v3.
- [61] Bolei Zhou, Aditya Khosla, Agata Lapedriza, Aude Oliva, and Antonio Torralba. Learning Deep Features for Discriminative Localization. Proceedings of the IEEE Computer Society Conference on Computer Vision and Pattern Recognition, 2016-December:2921-2929, 12 2015. ISSN 10636919. doi: 10.48550/arxiv.1512.04150. URL https://arxiv.org/abs/1512. 04150v1.

A Appendix

Following are presented the extended results and remarks about notation and nomenclature. In Table 2 are listed the evaluated abbreviated metric names followed by their source, categorized by the underlying explanatory quality they seek to assess [24]. Where applicable, IG-CAM and SG-CAM abbreviation have been used in place of Integrated Grad-CAM [45] and Smooth Grad-CAM++ [35] respectively. All results have been computed on a single A100-SXM4 80GB platform and a Xeon Gold 5317 with CUDA v12.0.

Table 2.	Nomenclature	of all the eva	lusted metrics	and their source
Table 2.	INDITIONALUIC	OI AII LIIC CVA	tuateu metites	and then source

	Acronym	Extended	Source
Faithfulness	F.E P.F Ins. Del. Ins-Del. IROF Suff. Inf.	Faithfulness Pixel Flipping Insertion AUC Deletion AUC Insertion-Deletion AUC IROF Sufficiency Infidelity	Alvarez-Melis and Jaakkola [7] Bach et al. [10] Petsiuk et al. [36] Petsiuk et al. [36] Englebert et al. [17] Rieger and Hansen [40] Dasgupta et al. [14] Yeh et al. [59]
Robustness	L. Est. M. Sens. A. Sens. RIS. ROS.	Local Lipschitz Estimate Max Sensitivity Avg. Sensitivity Relative Input Stability Relative Output Stability	Alvarez-Melis and Jaakkola [6] Yeh et al. [59] Yeh et al. [59] Agarwal et al. [4] Agarwal et al. [4]
Com.	CP. SP.	Complexity Sparseness	Bhatt et al. [11] Chalasani et al. [12]
Loc.	A.L. T-K.L. RR-A. RM-A.	Attribution Localization Top-K Intersection Relevance Rank Accuracy Relevance Mass Accuracy	Kohlbrenner et al. [30] Theiner et al. [57] Arras et al. [9] Arras et al. [9]
	R.T.	Running Time	

B Extended Quantitative Evaluation

We verified the effectiveness of our technique across a large set of metrics, datasets and benchmarking models to assess different explanatory qualities. Firstly, we quantified the *faithfulness* aspects by computing the *insertion* and *deletion* AUC(s) [36] on a large poolset. We then compare the results with respect to the *Faithfulness Estimate* [7], *Pixel Flipping* [10], *IROF* [40], *Sufficiency* [14] and *Infidelity* [59]. The *robustness* has been evaluated according to the *Local Lipschitz Estimate* [6], *Max-Sensitivity*, *Avg-Sensitivity* [59], *Relative Input Stability* (*RIS*), Relative Output Stability (ROS) [4]. The complexity characteristic has been measured according to the *Sparseness* [12] and *Complexity* criteria [11]. *Insertion* and *deletion* metrics have been computed using the IROF library [40], while the other metrics using the *Quantus* framework v0.4.4. [24]. **Notably.** *F.E* has been adopted for a more fair comparison as it is known to exhibit rank-order conflicts [41, 25] with similar metrics (*e.g. P.F*). Due to space constraints we have attached the extended results below. The attribution baseline methods Grad-CAM, Grad-CAM++, Smooth Grad-CAM++, XGrad-CAM, Layer-CAM, Score-CAM, for Integrated Grad-CAM the code from the official repository has been adopted.

In Table 3 are shown the extended *faithfulness* results across the three benchmarking models, while in Table 4 are presented the findings of the localization metrics. In Figure 7 is shown an example of a generated binary segmentation masks. As we employed a binary mask, the results of RM-A [9] are comparable to A.L [30] which we propose in table 5. The relative robustness (RIS/ROS) results are tabulated in table 6. Ultimately, the infidelity aspect has also been additionally verified on the CIFAR-10 and its results showed in table 7.

Table 3: Faithfulness Metrics: Insertion and Deletion [36] AUCs computed on 5000 samples of *ILSVRC2012* [42] on VGG16 [49], ResNet-50 [23] and AlexNet [31]. **Boldface values indicate best scores**.

	VGG16		ResNet-50			AlexNet			
Method	↑ Ins.	↓ Del	↑ Ins-Del.	↑ Ins.	↓ Del	↑ Ins-Del.	† Ins.	↓ Del	↑ Ins-Del.
Grad-CAM	0.60	0.09	0.51	0.86	0.21	0.65	0.50	0.17	0.32
Grad-CAM++	0.58	0.10	0.49	0.84	0.21	0.63	0.48	0.18	0.30
Smooth Grad-CAM++	0.44	0.17	0.27	0.74	0.30	0.45	0.36	0.28	0.09
Integrated Grad-CAM	0.61	0.09	0.52	0.86	0.21	0.65	0.51	0.17	0.34
HiRes-CAM	0.57	0.10	0.47	0.86	0.21	0.65	0.49	0.18	0.32
XGrad-CAM	0.62	0.09	0.53	0.86	0.2097	0.65	0.51	0.16	0.35
LayerCAM	0.57	0.10	0.47	0.83	0.22	0.61	0.47	0.19	0.28
Score-CAM	0.56	0.11	0.46	0.83	0.23	0.60	0.51	0.1522	0.3554
Ablation-CAM	0.57	0.10	0.48	0.85	0.21	0.64	0.50	0.17	0.33
Expected Grad-CAM	0.65	0.09	0.56	0.87	0.2093	0.66	0.52	0.1569	0.3556

Table 4: Localization Metrics: scores computed on 500 samples on the MS-COCO [32] dataset on VGG16 [49], ResNet-50 [23] and AlexNet [31]. Computed on labels "zebra" and "stop sign". **Boldface values indicate best scores**.

	VGG16			ResNet-50			AlexNet		
Method	↑ A.L.	↑ T-K.I.	↑ RR-A	↑ A.L.	↑ T-K.I.	↑ RR-A	↑ A.L.	↑ T-K.I.	↑ RR-A
Grad-CAM	0.11	0.24	0.24	0.09	0.11	0.12	0.09	0.07	0.1
Grad-CAM++	0.13	0.30	0.29	0.106	0.11	0.128	0.08	0.03	0.07
Smooth Grad-CAM++	0.10	0.18	0.19	0.07	0.11	0.12	0.08	0.03	0.06
Integrated Grad-CAM	0.12	0.34	0.31	0.097	0.119	0.13	0.08	0.07	0.1
HiRes-CAM	0.11	0.22	0.23	0.097	0.11	0.12	0.08	0.04	0.08
XGrad-CAM	0.11	0.24	0.24	0.09	0.11	0.12	0.08	0.05	0.08
LayerCAM	0.11	0.25	0.24	0.08	0.1	0.11	0.07	0.02	0.06
Score-CAM	0.12	0.25	0.23	0.09	0.118	0.132	0.109	0.17	0.15
Ablation-CAM	<u>0.15</u>	<u>0.36</u>	<u>0.33</u>	0.09	0.11	0.12	0.106	0.15	0.14
Expected Grad-CAM	0.18	0.42	0.36	0.104	0.18	0.17	0.13	0.23	0.18

Table 5: Localization Metrics: Rank Mass Accuracy [9] computed on 500 samples on the MS-COCO [32] dataset on VGG16 [49], ResNet-50 [23] and AlexNet [31]. Computed on labels "zebra" and "stop sign". **Boldface values indicate best scores**.

Table 6: Robustness Metrics: RIS/ROS [4] computed on 500 samples on the *ILSVRC2012* [42] dataset on VGG-16 [49] and ResNet-50 [23]. Methods marked with a '-' have been excluded due to zero-attribution values being produced under infinitesimal perturbations. **Boldface values indicate best scores**.

	VGG16	ResNet-50	AlexNet
Method	↑ RM-A	↑ RM-A	↑ RM-A
Grad-CAM	0.11	0.09	0.09
Grad-CAM++	0.13	0.11	0.08
Smooth Grad-CAM++	0.10	0.07	0.08
Integrated Grad-CAM	0.12	0.10	0.08
HiRes-CAM	0.11	0.10	0.08
XGrad-CAM	0.11	0.09	0.08
LayerCAM	0.11	0.08	0.07
Score-CAM	0.12	0.09	0.11
Ablation-CAM	<u>0.15</u>	0.09	0.11
Expected Grad-CAM	0.18	<u>0.11</u>	0.13

	VG	G-16	ResN	let-50
Method	↓ RIS	↓ ROS	↓ RIS	↓ ROS
Grad-CAM	169.197	5527.376	103.162	1.55e+04
Grad-CAM++	0.045	1.3	357.893	3130.042
Smooth Grad-CAM++	25.003	2.704	59.733	1180.478
Integrated Grad-CAM	-	-	-	-
Hi-Res CAM	-	-	-	-
XGrad-CAM	33.872	2812.874	111.022	1.65e+04
LayerCAM	0.023	33.782	11.712	555.22
Score-CAM	0.09	14.97	19.046	2053.248
Ablation-CAM	-	-	-	-
Expected Grad-CAM	0.004	0.12	0.573	73.934

Table 7: Faithfulness Metrics: Infidelity [59] computed on 500 samples on the CIFAR10 [26] dataset on VGG-16 [49], ResNet-50 [23] and AlexNet [31]. Samples have been upsampled to 96×96 and the *Infidelity* metric has been computed using a perturbation patch size of 32 instead of 56. Due to the sample low resolution, results' values are high. For readability all values have been divided by 1×10^7 , 1×10^8 and 1×10^9 for VGG-16, ResNet-50 and AlexNet respectively.

	VGG16	ResNet-50	AlexNet
Method	↓ Inf.	↓ Inf.	↓ Inf.
Grad-CAM	1592.0	94.2	594.6
Grad-CAM++	1506.5	88.9	542.0
Smooth Grad-CAM++	1673.5	82.9	479.0
Integrated Grad-CAM	1.64e + 09	3.79e+08	4.83e+08
Hi-Res CAM	1585.6	77.6	594.1
XGrad-CAM	1549.2	93.5	575.0
LayerCAM	1457.0	92.5	555.1
Score-CAM	1751.7	157.3	656.6
Ablation-CAM	1670.2	<u>76.5</u>	619.7
Expected Grad-CAM	4.7	3.8	9.6

Table 8: Running time computed on 100 sequential runs on the CIFAR10 [26] dataset on VGG-16. Averaged values are displayed.

Method	↓ R.T.
Grad-CAM	0.006
Grad-CAM++	0.006
Smooth Grad-CAM++	0.121
Integrated Grad-CAM	0.156
Hi-Res CAM	0.006
XGrad-CAM	0.006
LayerCAM	0.006
Score-CAM	0.261
Ablation-CAM	0.302
Expected Grad-CAM	0.115

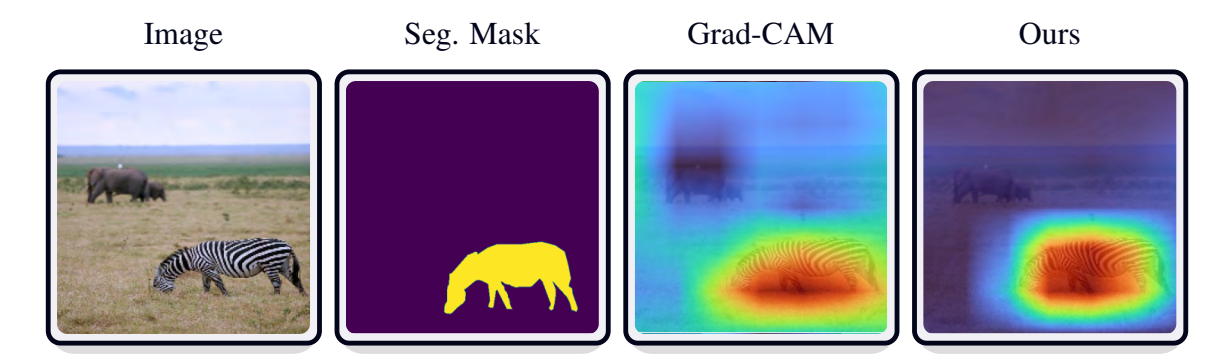


Figure 7: Example of generated binary segmentation mask for the label "zebra" from the MS-COCO dataset against Grad-CAM (baseline) and Expected Grad-CAM (our). Our technique retains and consistently exhibits low-noise properties on separate datasets.

B.1 Internal Saturation

Following [55] we evaluated the saturation at various points on modernly pretrained VGG-16 [49], ResNet-50 [23] and AlexNet [31]. In Figure 9a are shown the 25 random samples utilized, alongside a selected excerpt of the samples generated using the following feature scaling procedure (fig. 9b) for N=25:

$$\{\alpha_i \mid \alpha_i \sim U(0,1), i = 1, 2, \dots, N\}$$

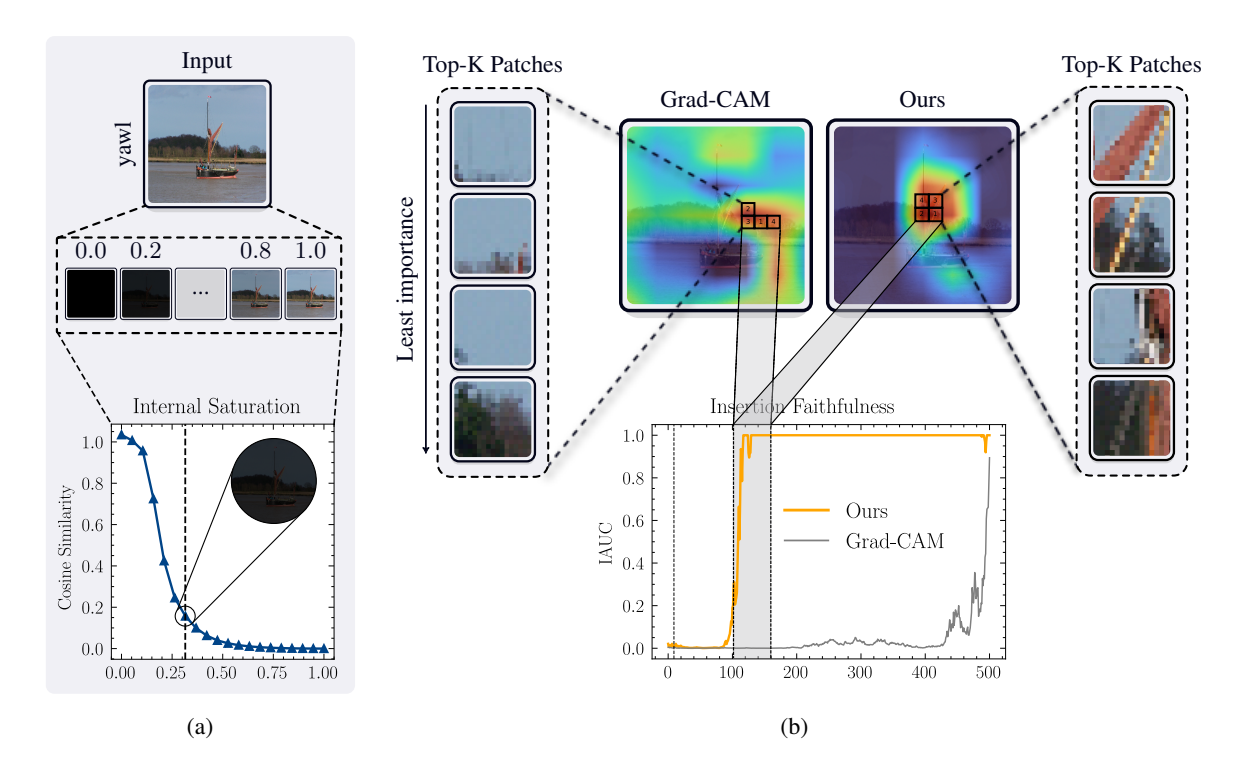


Figure 8: Comparison of the attribution maps under internal saturation conditions. In Figure 2a is shown the cosine similarity of the target layer's embeddings with respect to the interpolator parameter (α) . Figure 2b shows the attribution maps of the different methods under the saturation condition. The internal saturation condition causes the baseline method to under-represent feature importances across saturating ranges. By extracting the top-4 most important features (fig. 2b) we can observe that the baseline method fails to capture the relevant discriminative regions, which produce low insertion AUCs (fig. 2b) as deemed not important by the model.

Figures 10 and 11 shows the saturating behavior w.r.t. the output and intermediary layers targeted by CAM methods. Both the pre-softmax and post-softmax outputs quickly flatten and plateaus for very small value of the feature scaling factor α , with the softmax outputs showing the swiftest rate of change and abruptly converge to saturation (fig. 11). When selecting an arbitrary intermediary layer (i.e. the one targeted by the analyzed CAM methods) the saturation phenomena is still present but offset due to the reduced path (depth) (fig. 8). As α increases, the cosine similarity of the target layer's embeddings quickly flattens (Figure 8a), leading to an underestimation of feature attributions. This results in sparse, uninformative, and ill-formed explanations (Figure 8b). This is evident when inspecting the top-k most important patches according to the generated attribution maps, which focus on background areas rather than the target class (yawl). Consequently, when these patches are inserted, they produce low model confidence (Insertion IAUC) (Figure 8b). Conversely, our method focuses on salient discriminative areas of the image that characterize the target label (i.e. yawl) and highly activate the neural network, demonstrating high fidelity to the model's inner workings, robustness to internal saturation, and high localization by focusing only on the most important regions.

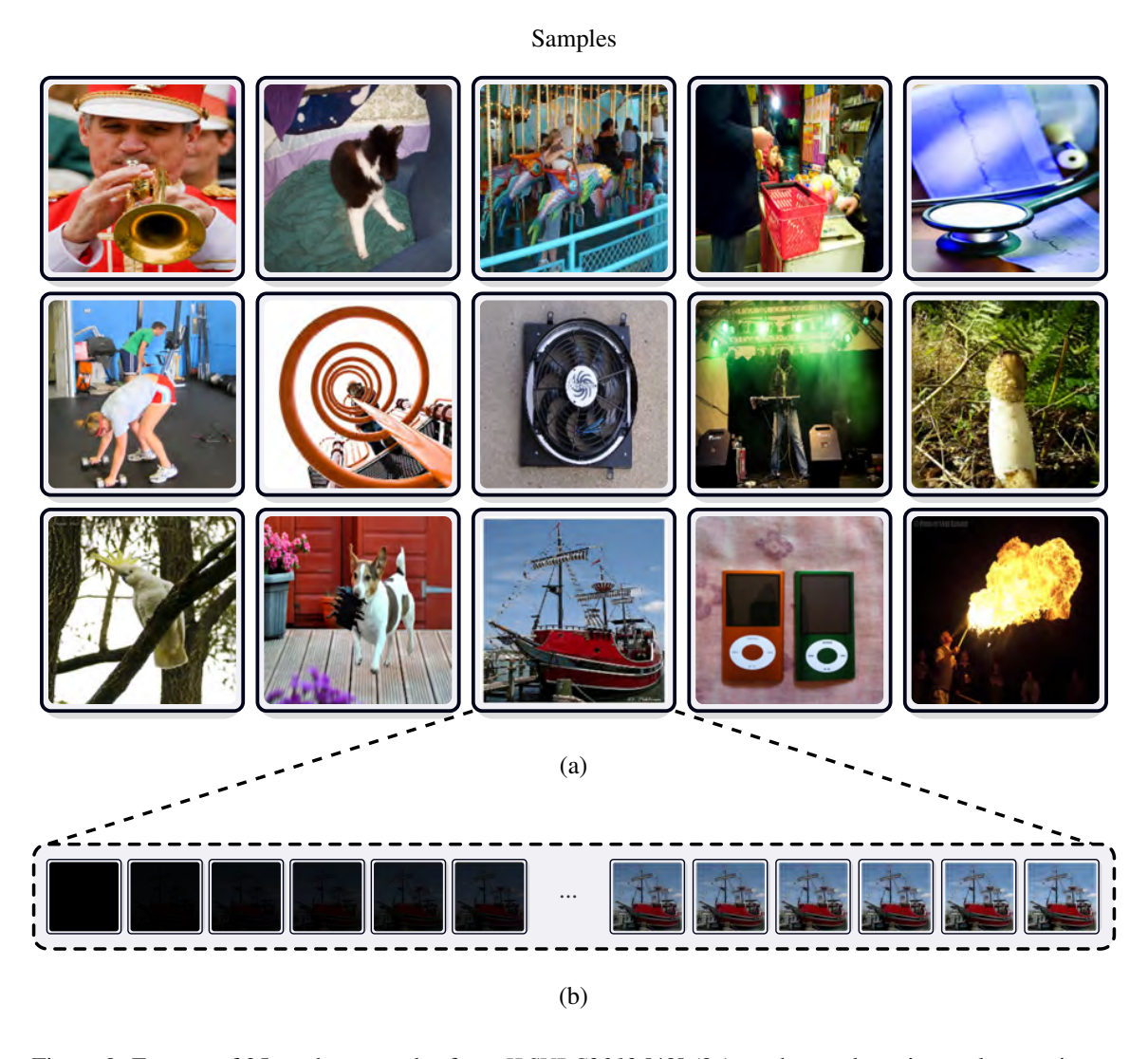


Figure 9: Excerpt of 25 random samples from *ILSVRC2012* [42] (9a) used to evaluate internal saturation at various points. Figure 9b presents a subset of samples generated through feature scaling over 25 steps.

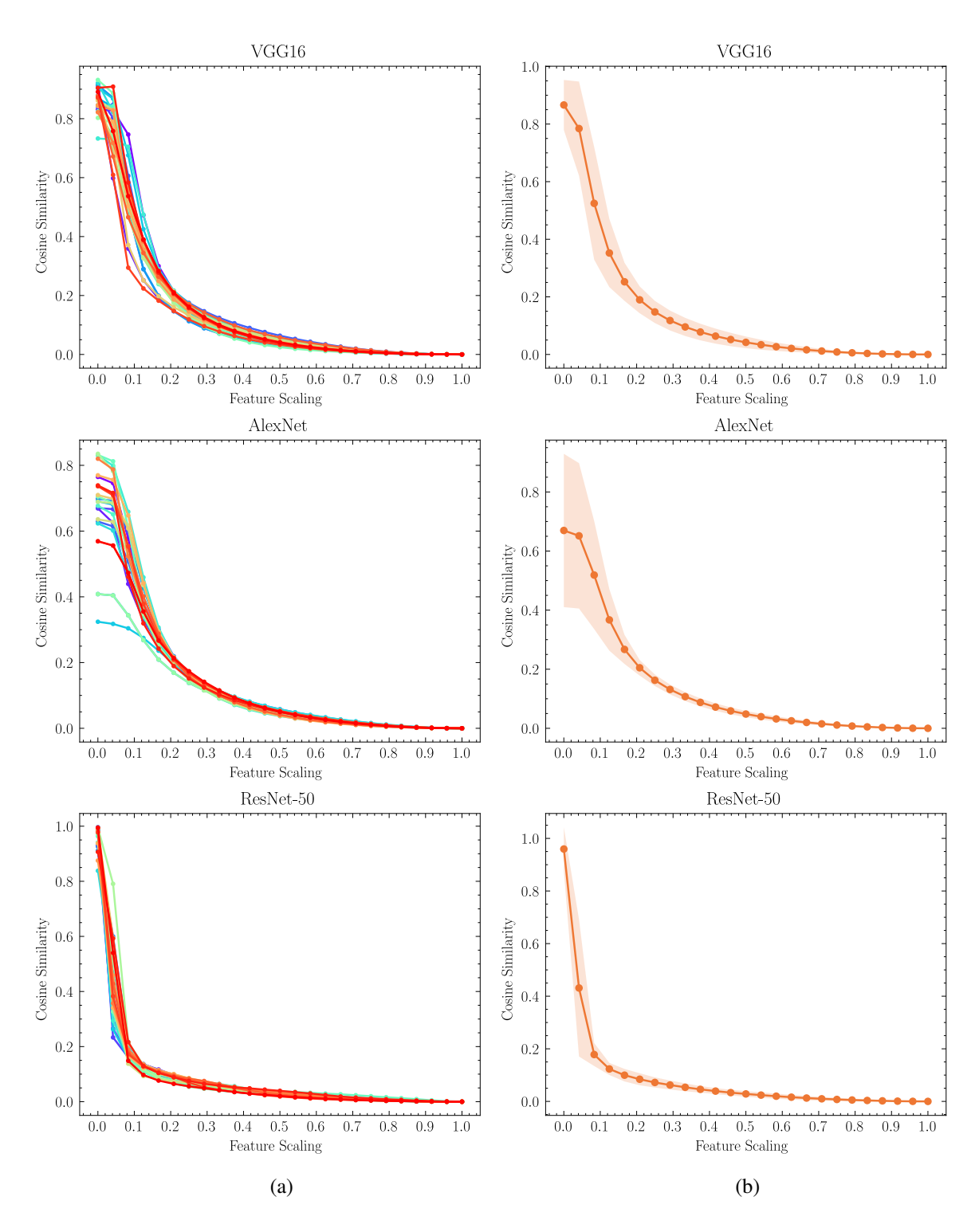


Figure 10: Internal saturation analysis of intermediary target layers in VGG16 [49], AlexNet [31], and ResNet-50 [23]. Figure 10a presents the cosine similarity between activation vectors of CAM target filters. Figure 10b depicts the mean values with error bars indicating 2 standard deviations. For VGG16 and AlexNet, the final feature layer is used, while for ResNet-50, the layer4 is selected.

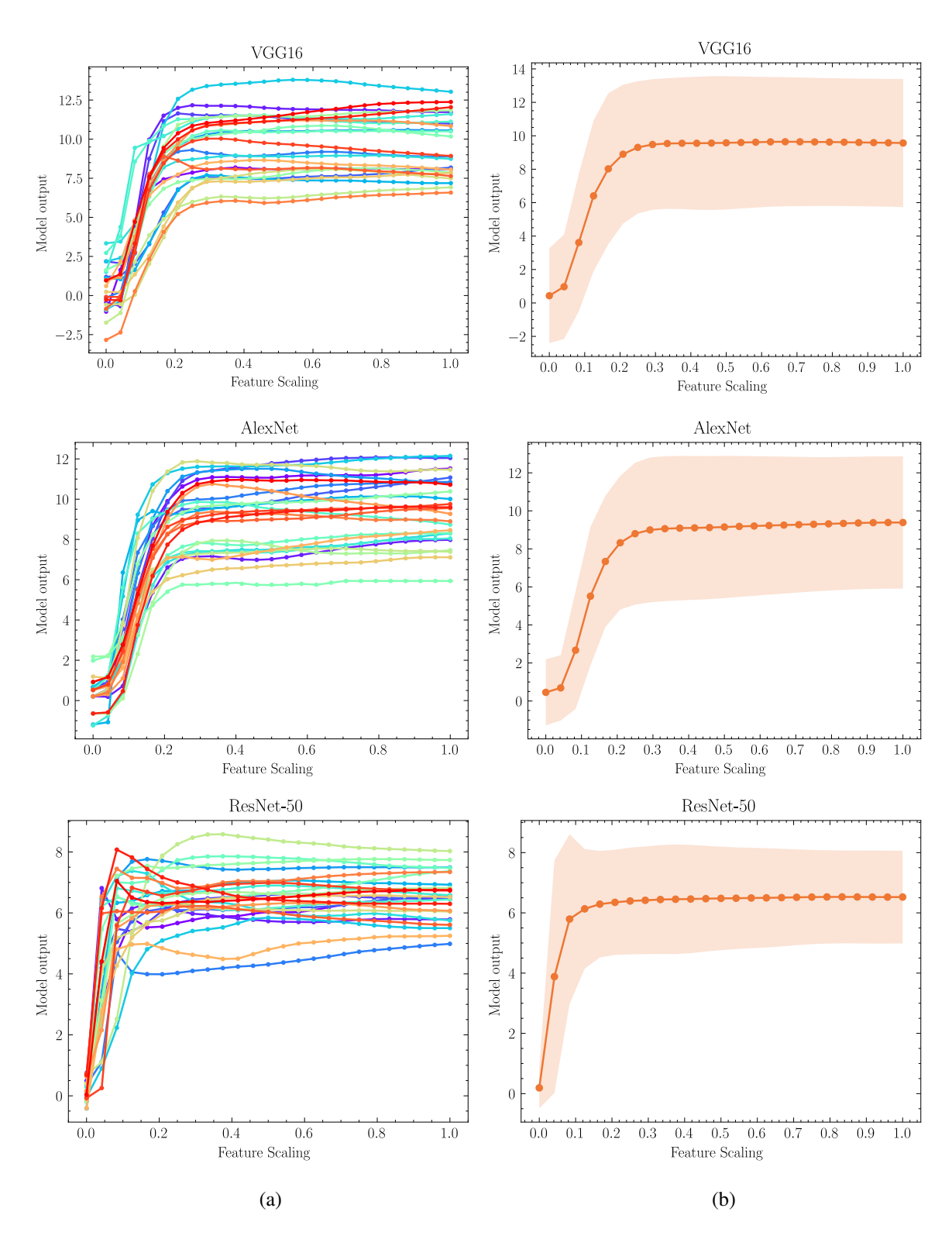


Figure 11: Output saturation analysis in VGG16 [49], AlexNet [31], and ResNet-50 [23] (fig. 11a). Figure 11a displays the softmax scores for the top label, while Figure 11b depicts the mean values with error bars indicating 2 standard deviations.

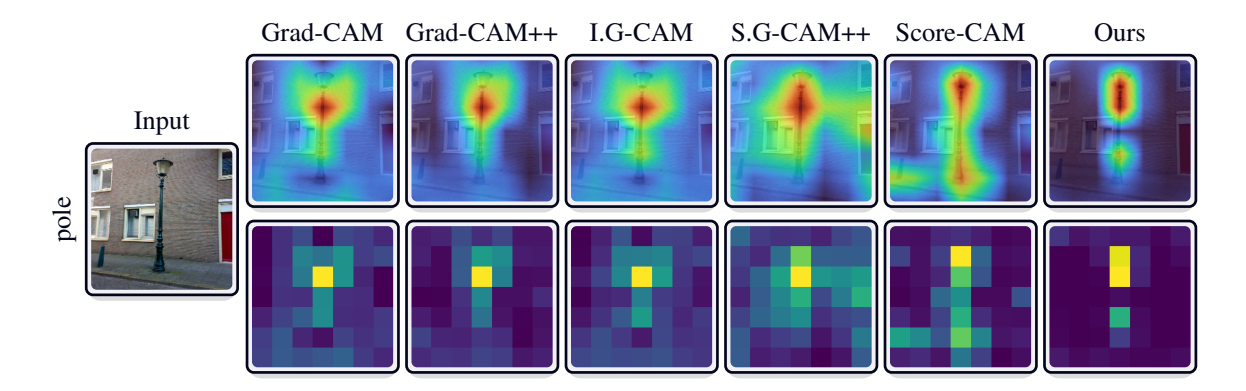


Figure 12: Gradients are noisy. A comparison of gradient-based CAM methods under optimal conditions shows that even recent methods exhibit high sensitivity.

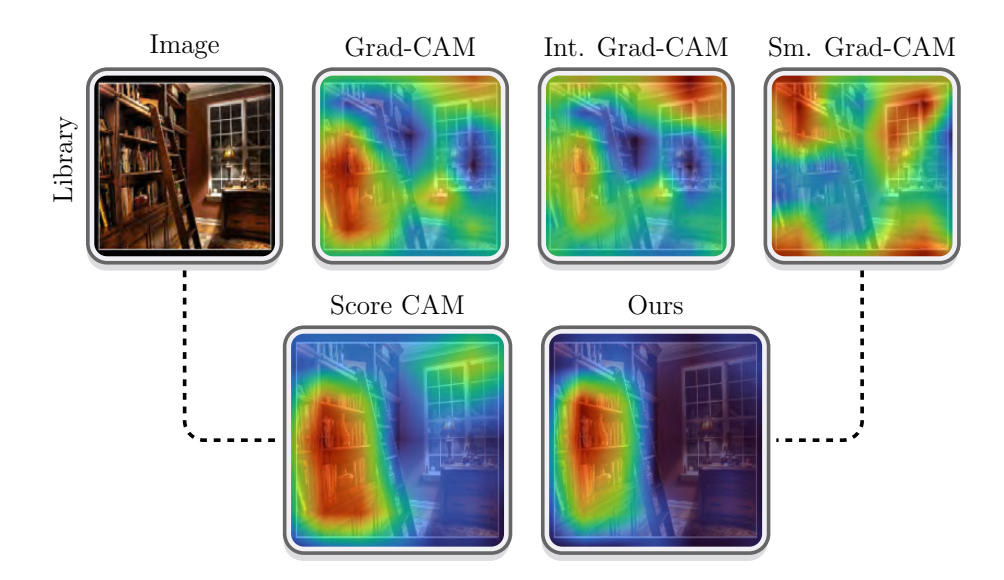


Figure 13: Comparison of gradient-based and non-gradient-based CAM methods. The top row illustrates the noisiness and tendency to produce ill-formed explanations in gradient-based methods, including recent approaches [45]. *Score-CAM* [58] addresses this issue by eliminating the use of gradients. Our method demonstrates the ability to generate sharper and more stable explanations consistently, even with the use of gradients.

C Qualitative Evaluation

Next we provide the extended version of all the figures *i.e.* including all the comparative baseline methods and some additional examples.

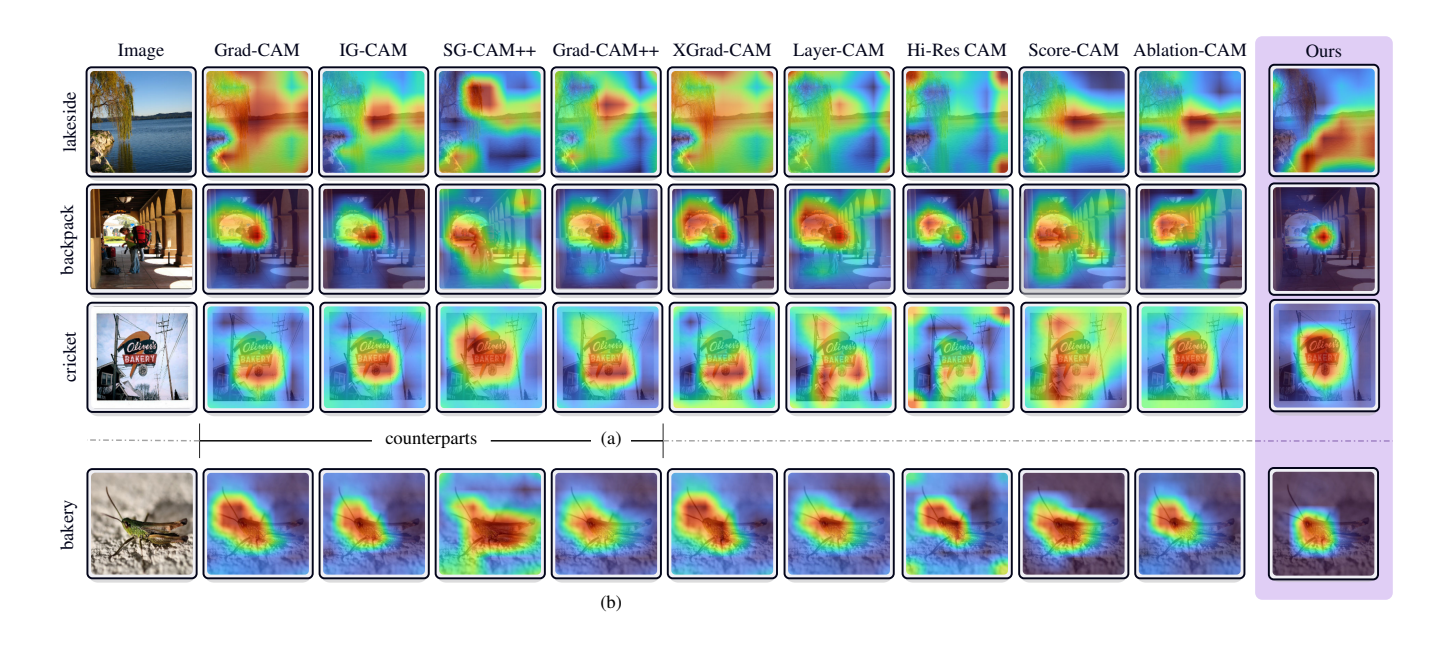


Figure 14: Comparison of the attribution maps for various methods under normal (14b) and internal saturation condition (14a). Extended version containing all baseline attribution methods.

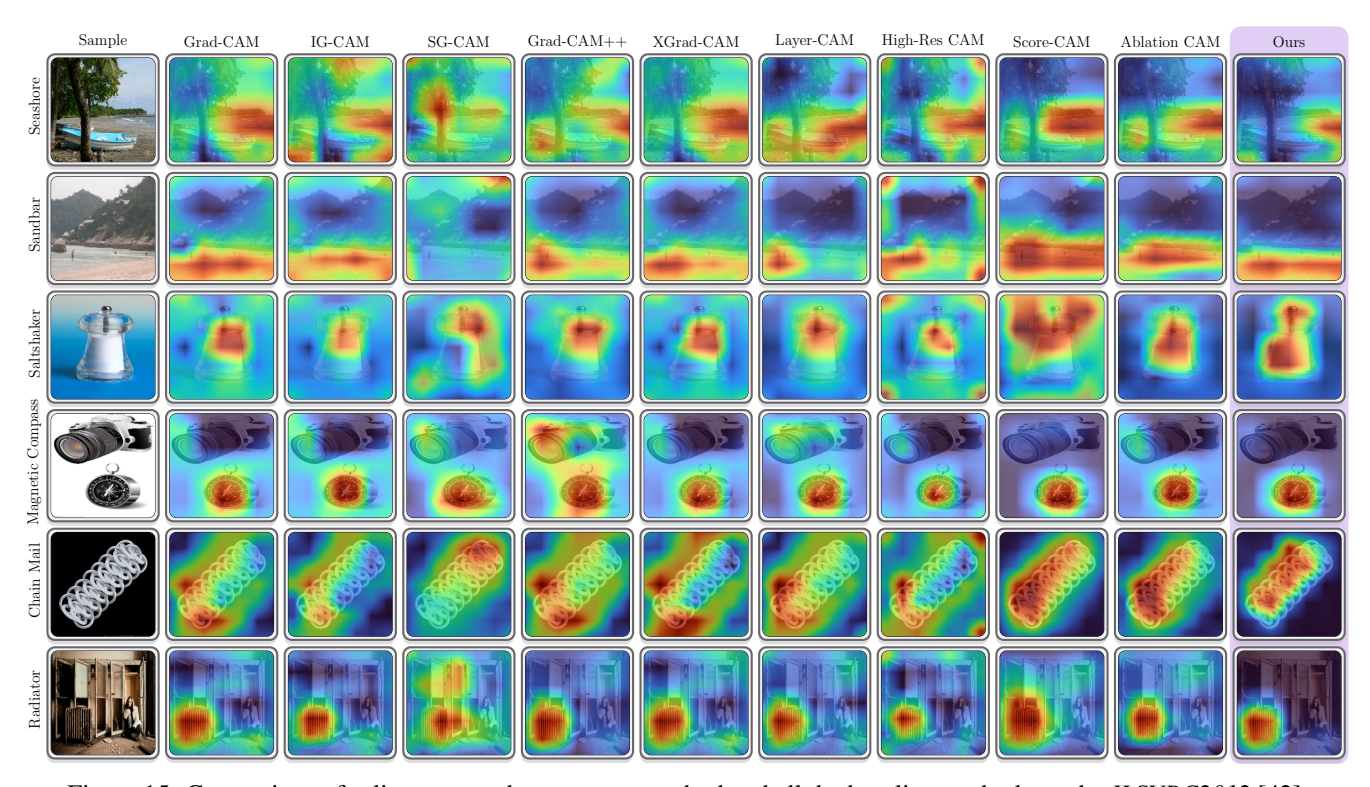


Figure 15: Comparison of saliency maps between our method and all the baseline methods on the ILSVRC2012 [42].